

Cell fine structure and phylogeny of *Parvodinium*: towards an ultrastructural characterization of the Peridiniopsidaceae (Dinophyceae)

Mariana S. Pandeirada ^{a,b}, Sandra C. Craveiro ^{a,b}, Niels Daugbjerg ^c, Øjvind Moestrup ^c
and António J. Calado ^{a,b}

^aDepartment of Biology, University of Aveiro, P-3810-193 Aveiro, Portugal; ^bGeoBioTec Research Unit, University of Aveiro, P-3810-193 Aveiro, Portugal; ^cMarine Biological Section, Department of Biology, University of Copenhagen, Universitetsparken 4, DK-2100 Copenhagen Ø, Denmark

ABSTRACT

Recent molecular phylogenies that include species of *Parvodinium* revealed as its closest relatives the genera *Peridiniopsis*, *Palatinus* and *Johsia*. The clade containing these taxa is currently recognized as a family, Peridiniopsidaceae. The affinity between the members of Peridiniopsidaceae cuts across traditional boundaries based on features of the amphiesma, most notably the presence or absence of an apical pore complex. Detailed descriptions of the fine structure of *Peridiniopsis* and *Palatinus* are available from TEM studies of their type species. Here we provide a description in comparable detail of a species of the *Parvodinium umbonatum–inconspicuum* complex, which includes the type of the genus. The cells had an apical fibrous complex essentially similar to those described from other peridinioids prepared with comparable fixations. The pusular system was extensive and included areas with different aspects: an area with a sheet-like vesicle along the mid-right side of the cell, a ventral portion with ramified and anastomosed tubes and a somewhat flattened tube attached to the transverse flagellar canal. The most remarkable feature was the microtubular strand that extended from a ventral, protruding peduncle to the anterior part of the epicone, around an accumulation body, and came around along a more dorsal position toward the ventral side. This long microtubular strand of the peduncle (MSP) was reminiscent of the one described from *Peridiniopsis borgei*, both by its extension and looping path, and by the breaking up of the strand of microtubules into smaller portions with a wavy appearance; and contrasted with the reduced MSP of *Palatinus apiculatus*. The fine-structural features currently known from Peridiniopsidaceae are summarized. Members of the family include a flagellar apparatus with four microtubule-containing roots associated, the basal bodies inserted close to each other, nearly at right angles and a three-armed fibrous connective between root 1 and the transverse basal body.

HIGHLIGHTS

- Detailed fine structure of *Parvodinium* (of *P. umbonatum–P. inconspicuum* complex).
- Comparative analysis of the ultrastructure of *Parvodinium* and other Peridiniopsidaceae.
- Summary of ultrastructural features of the family Peridiniopsidaceae.

ARTICLE HISTORY Received 3 December 2021; Revised 26 March 2022; Accepted 3 June 2022

KEYWORDS Dinoflagellates; flagellar apparatus; (microtubular strand of the) peduncle; peridinioid; Peridiniopsidaceae; phylogeny; pusule; SSU-ITS-LSU rDNA; ultrastructure

Introduction

Over the past decade, many freshwater dinoflagellates formerly classified in the family Peridiniaceae have been reassigned to the mainly marine family Thoracosphaeraceae (including the Pfiesteriaceae), based on similarity of plate pattern, intracellular organization and molecular data (Craveiro *et al.*, 2011, 2015, 2016; Moestrup & Calado, 2018). More recently, the family Peridiniopsidaceae was established to segregate from the Peridiniaceae three freshwater genera that consistently formed a well-supported clade in phylogenetic analyses based on ribosomal DNA sequences: *Peridiniopsis* Lemmermann, *Parvodinium* Carty and *Palatinus* Craveiro, Calado, Daugbjerg & Moestrup (Gottschling *et al.*, 2017). The new genus *Johsia* Z.Luo, Na Wang, K.N.Mertens & H.Gu, was

subsequently described from marine sediments of the Gulf of Thailand and off Manado (Indonesia), and added to the Peridiniopsidaceae (Luo *et al.*, 2020). Another marine peridinioid, described from tide pools, '*Scrippsiella*' *hexapraecingula* has been grouping in the phylogenetic trees with the Peridiniopsidaceae (Luo *et al.*, 2020). Members of the family display morphological diversity in aspects traditionally considered phylogenetically significant, such as the presence or absence of an apical pore. The amphiesmal arrangement of six plates in the cingulum and up to two anterior intercalary plates were suggested to be unifying features of the family (Gottschling *et al.*, 2017; Kretschmann *et al.*, 2018, 2019; Luo *et al.*, 2020). However, it is unclear which internal cell features

CONTACT Sandra C. Craveiro scraveiro@ua.pt

© 2022 British Phycological Society

may be considered characteristic of the group. Detailed fine-structural descriptions, including flagellar apparatus, pusular system and strands of microtubules related with a homology of a feeding apparatus, are available for the type species of *Peridiniopsis* (Calado & Moestrup, 2002) and *Palatinus* (Craveiro *et al.*, 2009) but only limited information has been published for *Parvodinium*, *Johsia* and ‘*Scrippsiella*’ *hexapraecingula* (Seo & Fritz, 2002; Horiguchi *et al.*, 1999; Luo *et al.*, 2020). Ultrastructural analyses of species of these genera are needed for a more complete characterization of the Peridiniopsidaceae. Ultrastructural studies of peridinioids (e.g. Calado *et al.*, 1999; Calado & Moestrup, 2002; Craveiro *et al.*, 2009) have shown that their flagellar apparatus usually includes two microtubular roots associated with the longitudinal basal body (LB): a strand of microtubules on the left side of the LB, the so-called longitudinal microtubular root (LMR or r1 in Moestrup, 2000) and a single microtubule, on the right side of the LB, the so-called single microtubular root (SMR or r2 in Moestrup, 2000). Associated with the transverse basal body (TB) there are two other roots: a single microtubule, the transverse microtubular root (TMR or r3 in Moestrup, 2000) that nucleates one or several rows of microtubules (TMRE, transverse microtubular root extension), and a fibre associated with a microtubule, the transverse striated root and transverse striated root microtubule (TSR+TSRM/r4 in Moestrup, 2000). Also characteristic of peridinioids is the presence of a layered connective (LC) that associates two of these roots (LMR/r1 and TSR+TSRM/r4), one associated to each of the basal bodies (e.g. Calado *et al.*, 1999; Craveiro *et al.*, 2015). In other groups of dinoflagellates, the LC is usually replaced by an elongated striated fibre (the striated root connective, SRC), which links the same two roots at a more distal position (e.g. Iwataki *et al.*, 2010; Pandeirada *et al.*, 2021).

The pusular system is often very complex and difficult to elucidate due to the variable extent, to which pusular elements collapse in response to different fixation schedules (e.g. Craveiro *et al.*, 2009). Despite these difficulties, the pusular system has shown enough regularity in some dinoflagellate groups to be considered characteristic of those groups. A typical example is the strict tubular organization of the pusules of species of Tovelliaceae, in which pusular tubes display a regular arrangement of diverticula along part of their length and electron-opaque structures associated with the inner membrane in other areas (Lindberg *et al.*, 2005; Calado, 2011).

Most of the photosynthetic peridinioids examined in detail with transmission electron microscopy (TEM) have either a single microtubular strand of the peduncle (MSP) or a more developed system, with up to eight partially overlapping rows of microtubules (microtubular basket, MB). The most extensive MBs are found in pfiesteriaceans, a group of predatory dinoflagellates that includes marine (e.g. *Paulsenella* and *Pfiesteria*; Schnepf *et al.*, 1985; Litaker *et al.*, 2002) and freshwater genera (*Tyrannodinium*; Calado & Moestrup, 1997), in which they play a role in food uptake (Hansen & Calado, 1999). In some freshwater members of the photosynthetic ‘calcareous’ clade, the Thoracosphaeraceae (e.g. *Chimonodinium lomnickii* and *Naiadinium polonicum* (Wołoszyńska) Carty; Craveiro *et al.*, 2011, 2013), a conspicuous MB is present but there is no evidence yet of food uptake in these species. The MSP is a more generally distributed structure that has been found in Borghiellaceae (*Baldinia anauniensis* Gert Hansen & Daugbjerg; Hansen *et al.*, 2007), Tovelliaceae (e.g. *Tovellia rubescens* Pandeirada, Craveiro, Daugbjerg, Moestrup & Calado; Pandeirada *et al.*, 2019), Suessiaceae (e.g. *Prosoaulax lacustris* (F.Stein) Calado & Moestrup; Calado *et al.*, 1998) and also in the Peridiniopsidaceae (e.g. *Peridiniopsis borgei*; Calado & Moestrup, 1997).

The genus *Parvodinium* includes freshwater peridinioid species with the plate formula: po, x, 4', 2a, 7", 6c, 5(?)s, 5"', 2'''' (Moestrup & Calado, 2018). About 16 species are currently recognized in this genus, but species identification can be quite difficult due to the small size of the cells, the similarity between described species and the variations of plate tabulation within species (Elbrächter & Meyer, 2001; Carty, 2008; Moestrup & Calado, 2018; Kretschmann *et al.*, 2018, 2019; Luo *et al.*, 2020). In particular, the identity of the type species of *Parvodinium*, *P. umbonatum* (F.Stein) Carty (= *Peridinium umbonatum* F.Stein) has been difficult to ascertain. The concept of *P. umbonatum*, as given in one of the most influential monographs that includes this group of taxa (Lefèvre, 1932), depicts it as so closely related to the species *Parvodinium inconspicuum* (Lemmermann) Carty (= *Peridinium inconspicuum* Lemmermann) that the two species were considered synonyms by Popovský & Pfiester (1986, 1990). The existence of a number of infraspecific taxa described in both these species further complicates the matter. However, populations identifiable as members of the complex *P. umbonatum*–*P. inconspicuum* can be easily found in different environments and often display minor differences in size, tabulation, or the presence of spines. This variability among populations, which suggests the existence of several species, was

the basis for keeping *P. inconspicuum* separate from *P. umbonatum* in the latest freshwater dinoflagellate flora (Moestrup & Calado, 2018). The recent description of taxa in this species complex demonstrated a higher species-level diversity than was previously recognized (Kretschmann *et al.*, 2018).

A dinoflagellate strain isolated from fresh water in the Buçaco mountain, Central Portugal, revealed features that place it in the *P. umbonatum*–*P. inconspicuum* complex; this was confirmed by phylogenetic analyses based on rDNA sequences. The fine structure of this strain was studied in detail and compared with the features of a Danish population with similar morphology.

Materials and methods

Sampling and establishment of cultures

The *Parvodinium* strain described here comes from a freshwater tank in the gardens of the Buçaco Palace Hotel (40°22'33.74"N, 8°21'55.62"W; ~380 m altitude), Buçaco mountain, Central Portugal. A swimming cell, from a net sample (mesh size 25 µm) collected on 7 July 2015, was isolated into a 96-well cell culture plate (Sarstedt, Numbrecht, Germany) with L16 medium (Lindström, 1991); and grew into a culture maintained at 18°C with 12h:12h light:dark photoperiod and photon flux density ca. 25 µmol m⁻² s⁻¹. Cells from this culture were transferred to DY-V medium (Andersen *et al.*, 1997) as they stopped growing in medium L16 and the culture was re-established under the same temperature, photoperiod and light intensity.

Cells of the *Parvodinium umbonatum*–*P. inconspicuum* species complex were isolated from a net sample collected in Gribso, Hillerød, Denmark, on 7 October 1996, and prepared for TEM (see below).

The phylogenetic analyses included a new sequence of *Parvodinium elpatiewskyi* (Ostenfeld) Kretschmann, Zerdoner & Gottschling, a species recently included in the Peridiniopsidaceae. The analysed strain was collected from a system of shallow, freshwater lakes in Gafanha da Boavista, Ílhavo, Aveiro (40°36'13.54"N, 8°41'49.17"W). A swimming cell of *P. elpatiewskyi* was isolated from a net sample collected on 29 September 2017 and originated a culture from which rDNA was extracted. Cells in the culture divided slowly in quadruple concentration L16 medium (Lindström, 1991) at the same temperature, photoperiod and light intensity as above. The strain was characterized morphologically (Supplementary figs S1–S4) before the culture was lost.

Light microscopy (LM)

Swimming cells and empty thecae from Portuguese *Parvodinium* cultures were photographed with a ColorView IIIu Olympus camera (Olympus, Tokyo, Japan) mounted on a Zeiss Axioplan 2

imaging light microscope (Zeiss, Oberkochen, Germany). Images showing the position of the nucleus in cells of *Parvodinium* from Buçaco that sunk to the bottom of culture wells were recorded with a JVC TK-C1481BEG colour video camera (Norbain SD, Reading, UK) mounted on a Leitz Labovert FS inverted light microscope (Leica Microsystems, Wetzlar, Germany).

Scanning electron microscopy (SEM)

A volume of 600 µl from Buçaco culture was fixed for 1 h with 320 µl of a fixing mixture of 2% osmium tetroxide and saturated HgCl₂ (3:1, v/v). Fixed material was retained on Nuclepore polycarbonate filters with 5-µm pore size (Whatman, GE Healthcare Life Sciences, Maidstone, UK) that were washed with distilled water, dehydrated through a graded ethanol series and critical-point-dried in a Baltec CPD-030 (Balzers, Liechtenstein). The filters were glued onto stubs, sputter-coated with gold-palladium and examined with a JEOL JSM 6335F scanning electron microscope (Jeol, Tokyo, Japan) at University of Copenhagen.

Transmission electron microscopy (TEM)

Fixation of the *Parvodinium* strain from Buçaco followed two protocols, which differed only in the fixative mixture: (1) a mixture of 1% glutaraldehyde and 0.5% osmium tetroxide (final concentrations), both in phosphate buffer 0.1 M, pH 7.2; and (2) 2% glutaraldehyde in the same buffer. In both cases, swimming cells were transferred to a watch glass with the fixative. After ca. 1 h 20 min of fixation the cells were washed in phosphate buffer, incorporated into 1.5% agar blocks and postfixed for 2 h with 1% osmium tetroxide in phosphate buffer. The agar blocks with the cells were washed in phosphate buffer followed by distilled water, dehydrated through a graded ethanol series and propylene oxide, and embedded in Agar 100 low viscosity resin (Agar Scientific, Stansted, Essex, UK). Cells were sectioned with a diamond knife in a Leica EM UC6 ultramicrotome. Ribbons of serial sections (70 nm thickness) were picked up with slot grids and transferred to Formvar film. They were contrasted with uranyl acetate and lead citrate. Serial sections of two cells were examined with a JEOL JEM 1010 electron microscope with a Gatan Orius digital camera (Gatan, Pleasanton, USA) at University of Copenhagen.

Swimming cells of *Parvodinium umbonatum*–*P. inconspicuum* complex were picked up from a sample collected in Gribso, Denmark, and fixed for 20 min in 2% glutaraldehyde in sodium cacodylate buffer 0.1 M, pH 7.4. The rest of the procedure was similar to that described above, except for the use

of sodium cacodylate buffer for washing and Spurr resin (TAAB, Aldermaston, England) for embedding.

DNA extraction and PCR amplifications of SSU, ITS and LSU rDNA

DNA of the Buçaco strain of *Parvodinium* was extracted from a pellet obtained from centrifuging 0.5 ml of culture at 200 rpm for 10 min, in a Universal 16 A centrifuge (Hettich Zentrifugen, Tuttlingen, Germany). The pellet was transferred to 100 µl of the extracting solution QuickExtract™ FFPE DNA Extraction Kit (epicentre, Illumina, San Diego, California) and the kit instructions were followed. Two microlitres of the extracted DNA were used in the first PCR amplification of LSU rDNA, and one microlitre of the amplified product was used in a nested-PCR; the primers and thermal profiles for both amplifications are the same as in Pandeirada *et al.* (2014, 2017). For SSU rDNA and ITS amplifications, 2 µl of extracted DNA were used with the same primers and thermal profile as in the second round of amplification described in Takano & Horiguchi (2005). The amplified rDNA was purified with the QIAquick PCR Purification Kit (Qiagen, Hilden, Germany) and sent to MacroGen Europe (Amsterdam, the Netherlands) for sequencing with the same primers used for PCR amplifications.

DNA was extracted from 50–70 swimming cells of *P. elpatiewskyi* culture and used in PCR amplifications of rDNA (SSU, ITS and LSU), following the steps described for species of *Sphaerodinium* in Pandeirada *et al.* (2021). The purified DNA was sent for sequencing at MacroGen Europe.

Alignment and phylogeny

The phylogenetic position of the Buçaco strain of *Parvodinium* was inferred from analyses of nuclear-encoded LSU rDNA gene sequences and concatenation of SSU rDNA, ITS1 and ITS2, 5.8 rDNA and LSU rDNA. The LSU rDNA data matrix (1667 bp including introduced gaps) comprised 54 genera of dinoflagellates and a total of 90 taxa. The LSU rDNA sequences of three ciliates, four Apicomplexa and *Perkinsus* were also included and formed the outgroup. This diverse assemblage of Alveolata was aligned using Muscle with default settings as implemented in JALVIEW (ver. 2.10.3b1, Waterhouse *et al.*, 2009). The aligned sequences were analysed using two methods: Bayesian inference and Maximum likelihood. For Bayesian inference we used MrBayes (ver. 3.2.5 x64, Ronquist & Huelsenbeck, 2003) and for Maximum likelihood PhyML (ver. 3, Guindon *et al.*, 2010). Bayesian analysis was conducted on a local computer with 5 million generations and a tree was sampled every

1000 generations. The burn-in value was evaluated by plotting the LnL values as a function of generations in a spreadsheet. It occurred after 501 generations (conservative number) and therefore 4500 trees were used for generating a 50% majority-rule consensus tree in PAUP* (ver. 4.0a build 169, Swofford, 2002). Maximum likelihood with 1000 bootstrap replications used the general time-reversible (GTR) substitution model and the option 'free rates' as the model for rates across sites. PhyML was run through the online version available on the Montpellier bioinformatics platform.

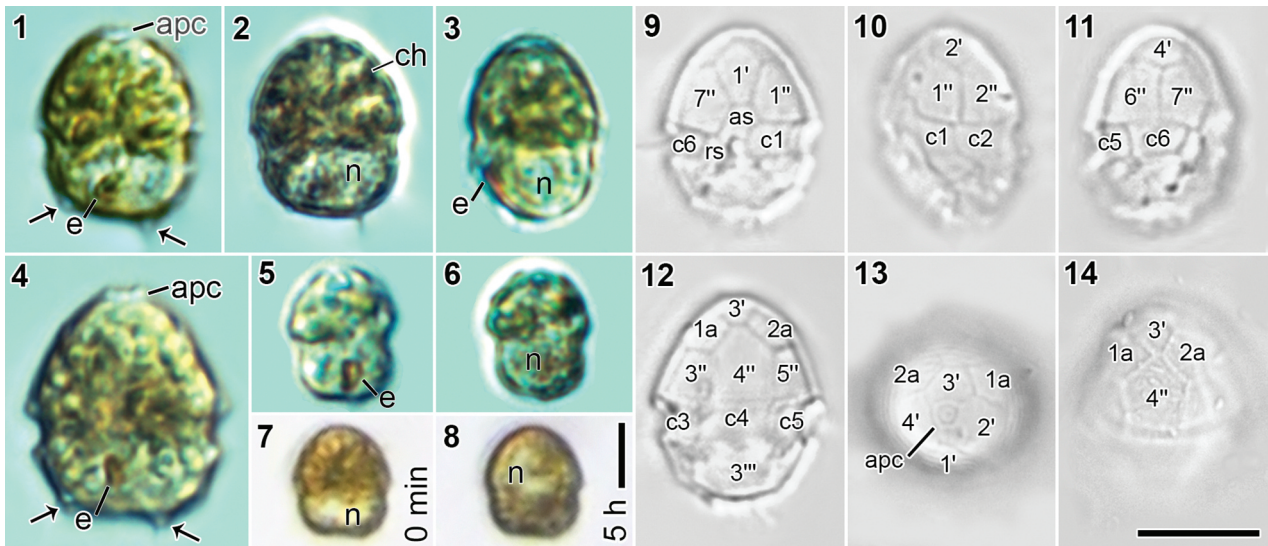
Based on the phylogenetic tree from analyses of LSU rDNA sequences, a concatenated data matrix comprising lineages of closely related dinoflagellates were prepared. The concatenated matrix comprised 3923 bp including introduced gaps. The ingroup included 11 genera and 21 species (including the Buçaco strain of *Parvodinium* and *P. elpatiewskyi*) whereas *Heterocapsa* spp. formed the outgroup. Sequence alignment and phylogenetic inference followed the same approach as outlined above for LSU rDNA. However, attempting a more accurate model of sequence evolution the genetic markers (coding and non-coding) were divided into five data partitions (SSU rDNA, ITS1, 5.8S rDNA, ITS2 and LSU rDNA). Hence, each region could evolve under different models of evolution using the 'unlink' option in MrBayes.

Results

Cell description from LM and SEM observations

Motile cells and empty thecae of the *Parvodinium* strain from Buçaco are shown in Figs 1–23. Cells were ovoid and slightly compressed dorsoventrally (Figs 1–3, 9–13, 15–19). The epicone was semi-elliptical to conical and larger than the hemispherical to trapezoidal hypocone (Figs 1, 2, 7–12, 15–18). The cingulum descended about half of its width, and the sulcus invaded slightly onto the epicone and widened markedly toward the antapex (Figs 9–11, 15, 16, 20, 21). The apical pore complex (apc) was visible in ventral or dorsal view, protruding slightly at the apex (Figs 1, 4, 9, 15–18). Cells were 17.4 ± 2 µm long (range 10.5–21 µm; $n = 68$), 12.2 ± 1.5 µm wide (range 6.5–15 µm; $n = 52$) and 10.4 ± 1.2 µm thick (range 7.5–12.5 µm; $n = 16$). Individual measurements are presented in Supplementary table S1. Larger cells had a more angular shape (Fig. 4), and the smallest were roughly circular to slightly elongated (Figs 5, 6). No cysts were observed in the cultures.

Chloroplast lobes were golden or yellowish-brown, densely arranged in the epicone and appeared radiating from a central area in some cells; no central



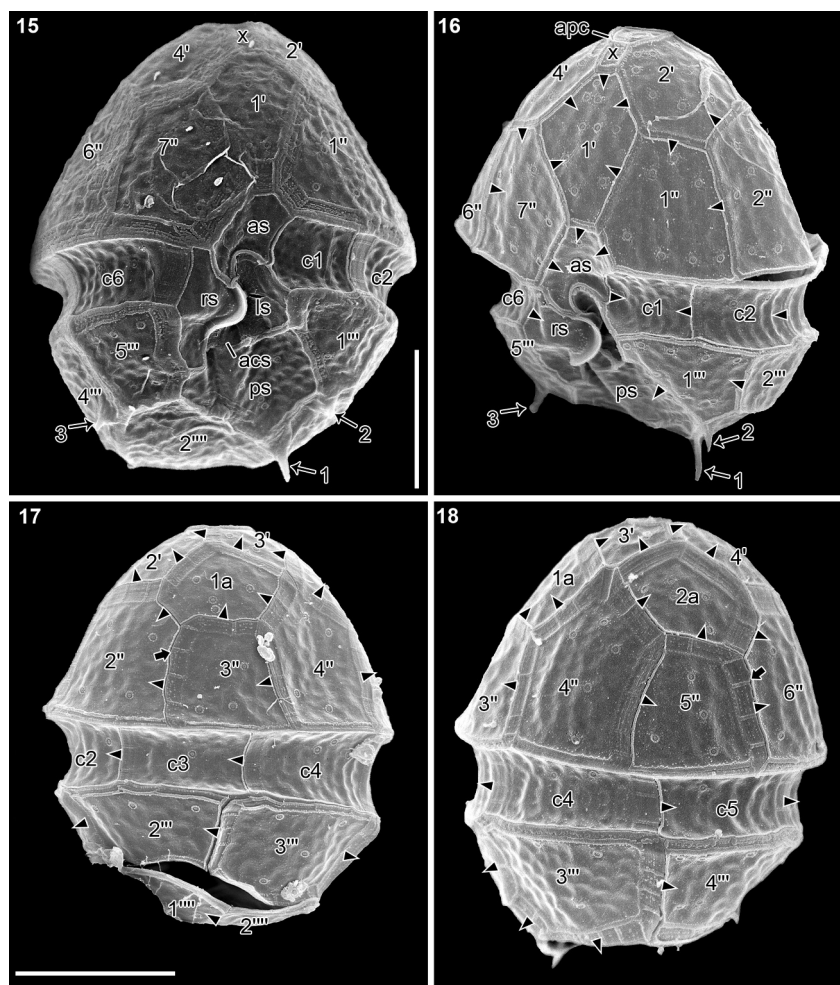
Figs 1–14. *Parvodinium* strain from Buçaco; LM of vegetative cells (**Figs 1–8**) and empty thecae (**Figs 9–14**). **Fig. 1.** Ventral view in surface focus showing the apical pore complex (apc), the eyespot (e) in the sulcus, and the position of two antapical spines (arrows). **Fig. 2.** Optical section of the same cell as in Fig. 1 with the nucleus (n) in the hypocone and the chloroplast lobes (ch) in the epicone. **Fig. 3.** Lateral view of a slightly dorsoventrally compressed cell. **Fig. 4.** Ventral view in surface focus of a larger cell with an angular outline. **Figs 5, 6.** Surface focus and optical section of a small, slightly elongated cell showing the eyespot (e) and the nucleus (n), respectively. **Figs 7, 8.** Still frames from a video recording made in an inverted microscope, of a small immobile cell, taken with 5 h interval, depicting the movement of the nucleus (n) towards the epicone. **Figs 9–11.** Empty thecae in ventral, left and right views showing Kofoidian notation of some plates. **Figs 12, 13.** Dorsal and apical views of two thecae with 3'-4''-conjunctum arrangement of plates. **Fig. 14.** Dorsal-anterior view with 3'-4''-contactum arrangement of plates. as and rs, anterior and right sulcal plates. Scale bars: **Figs 1–6, 9–14** same scale as in **Fig. 14**, 10 μ m; **Figs 7, 8** to the same scale, 10 μ m.

pyrenoid was noted (**Figs 1–6**). The nucleus was roundish to transversely elongated and occupied the hypocone up to about the cingulum level (**Figs 2, 3, 6**). In some immobile cells lying at the bottom of culture wells the nucleus was seen to move towards the epicone in a process that took up to 5 hours (**Figs 7, 8**). A nearly rectangular eyespot, sometimes somewhat tilted, 2.5–3.5 μ m long ($n = 10$), was seen in the sulcus (**Figs 1, 3–5**). In smaller cells, the eyespot overlapped a large portion of the sulcus (**Fig. 5**).

The tabulation observed was (Kofoidian notation): po, cp, x, 4', 2a, 7'', 6c, 5s, 5''', 2'''. The epitheca included four apical and seven precingular plates, and two anterior intercalary plates (1a, 2a) on the dorsal side (**Figs 9–19, 21**). The anterior intercalary plates were, in most cases (64% of the cells; $n = 50$), separated from each other, with the third apical plate sharing a suture with the fourth precingular plate: a 3'-4''-conjunctum arrangement (**Figs 12, 13, 19**). In fewer cases (36% of the cells; $n = 50$), the intercalary plates were closer to each other and plates 3' and 4'' barely touched: a 3'-4''-contactum arrangement (**Figs 14, 17, 18**). The apical pore complex (apc) consisted of three plates: a central cover plate (cp), encircled by the pore plate (po), which showed a closed suture on the ventral side where the nearly rectangular canal (marked x) plate abutted (**Figs 13, 16, 19, 22**).

On the hypotheca, the first antapical plate (1''') was smaller than the second (2'''), and there were five postcingular plates, of which plates 1''' and 5''' were the smallest (**Figs 15, 20, 21**). The cingulum included six plates of similar size except for the first that was somewhat shorter (**Figs 9–12, 15–18**). The sulcus included five plates: the anterior sulcal plate (as) slightly penetrated the epitheca; the posterior, and larger, sulcal plate (ps) extended to the antapex; the right sulcal plate (rs) extended into a flap that covered the exit pores of the flagella and the peduncle, and partly overlapped both the left sulcal (ls) and the smaller accessory (acs) plates (**Figs 15, 16, 20, 21, 23**). An extruded peduncle ca. 4 μ m long and 1.5 μ m wide was visible in SEM (**Figs 21, 23**).

Three spines were regularly seen projecting from the edges of the antapical plates (**Figs 1, 2, 4, 15, 16, 20, 21**). The largest was 1.5–2.1 μ m long and projected from plate 1''' near the corner with plates ps and 2''' (spine marked 1 in **Figs 15, 16, 20, 21**). A smaller spine, ca. 1 μ m long, was usually present on plate 1''' where it contacted plates ps and 1''' (marked 2 in **Figs 15, 16, 20, 21**); and another small spine projected from plate 2''' near the corner abutting plates 4''' and 5''' (marked 3 in **Figs 15, 16, 20, 21**). Shorter spines were seen irregularly along antapical sutures (e.g. spine marked 4 in **Fig. 21**).



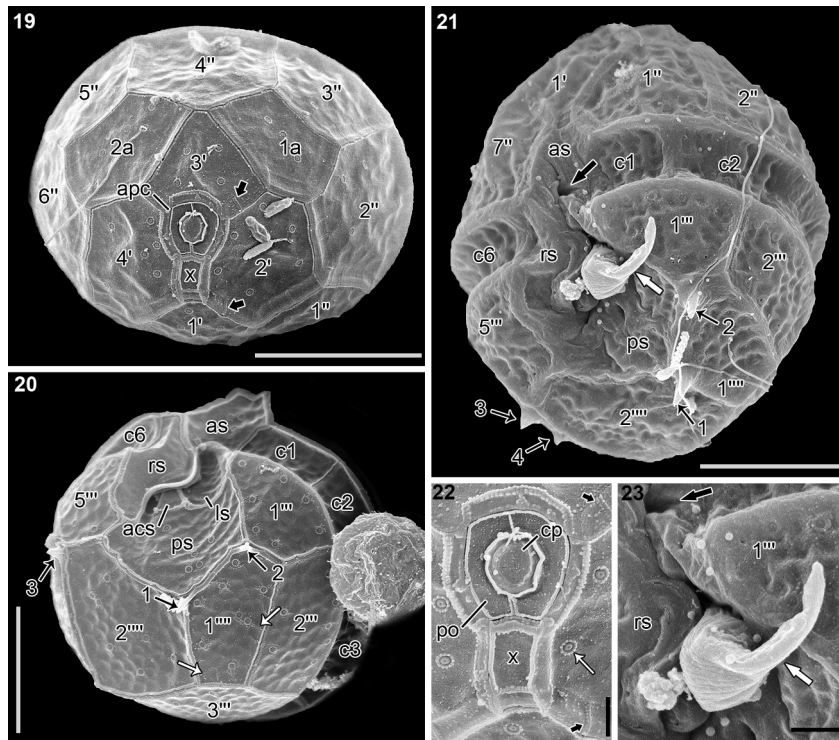
Figs 15–18. *Parvodinium* strain from Buçaco, SEM. Kofoidian notation. **Figs 15, 16.** Ventral and ventral-left views showing the five sulcal plates: anterior sulcal plate (as), right sulcal plate (rs), left sulcal plate (ls), posterior sulcal plate (ps) and the accessory sulcal plate (acs). The antapical spines are numbered 1 to 3. The apical pore complex (apc) is visible in **Fig. 16**. **Figs 17, 18.** Dorsal-left and dorsal-right views of thecae with wide striated sutures (arrows). Arrowheads in **Figs 16–18** indicate the direction of plate overlap. Scale bars: **Fig. 15**, 5 μm ; **Figs 16–18** to the same scale, 5 μm .

The plate surface was generally smooth, with the appearance of a faint reticulation when seen in SEM (**Fig. 20**, white arrows). Trichocyst pores were present throughout the cell surface but were absent from sutures and were not seen in the apc nor in right and left sulcal plates; each pore was surrounded by about a dozen small knobs, each about 40 nm in diameter (**Figs 15–20, 22**). Some, presumably older cells, showed wide sutures, up to over 1 μm , which were distinctly striated (**Figs 17–19, 22**, short black arrows). Plate overlap is indicated in **Figs 16–18**, marked with arrowheads. The tendential direction of overlapping was from dorsal to ventral side in the epitheca, cingulum and hypotheca. The plates that overlapped all the neighbour plates (keystone plates) were plate 4''' in the epitheca, plate 3''' in the hypotheca and plate c4 in the cingulum.

General cell ultrastructure (TEM)

The three cells analysed by TEM revealed similar fine-structural features (Supplementary figs S5–S19,

Figs. 24–44). General ultrastructural aspects are summarized in Supplementary figs S5, S12, S13, S17. Chloroplast lobes (ch) radiated from a central area near the base of the epicone and extended along the surface in the peripheral cytoplasm (Supplementary figs S5, S13, S17). Although some chloroplast lobes had thylakoid-free areas (Supplementary fig. S5, arrows), no pyrenoid complex was detected. Oil droplets (O), starch grains (st) and trichocysts (t) were seen at the cell periphery (Supplementary fig. S5). A distinct accumulation body (ab) was present on the anterior-left side of the epicone (Supplementary fig. S13). Pusular tubes and vesicles were visible along the longitudinal axis of the cell, but especially in the mid-ventral area (Supplementary fig. S5, pu). A cytoplasmic extension limited by a single membrane is shown outside the cell, near the sulcus, in Supplementary figs S5, S17. This so-called peduncle was supported by a microtubular strand (MSP) and contained round, electron-opaque bodies (Supplementary figs S5, S6, S17). An eyespot of type



Figs 19–23. *Parvodinium* strain from Buçaco, SEM. Kofoidian notation. **Fig. 19.** Apical view of a theca with wide striated sutures (arrows); apc, apical pore complex. **Fig. 20.** Antapical view showing two antapical plates of different size and five postcingular plates. The antapical spines are numbered 1 to 3. The sulcal plates are visible: anterior sulcal plate (as), right sulcal plate (rs), left sulcal plate (ls), posterior sulcal plate (ps) and the accessory sulcal plate (acs). All plates have a reticulated ornamentation (white arrows). **Fig. 21.** Ventral-antapical view of a cell with a peduncle protruding from the sulcus (large white arrow); the exit-pore of the transverse flagellum (large black arrow) is visible. An extra antapical spine is present (numbered 4). **Fig. 22.** Apical pore complex (apc), comprising pore plate (po), cover plate (cp) and canal plate (x). Trichocyst pores surrounded by small knobs (white arrow) and striation in the wide sutures are visible (short black arrows). **Fig. 23.** Detail of Fig. 21, showing the exit-pore of the transverse flagellum (black arrow) and the peduncle (white arrow). Scale bars: Figs 19–21, 5 μ m; Fig. 22, 500 nm; Fig. 23, 1 μ m.

A (Moestrup & Daugbjerg, 2007) was located beneath the sulcus, and comprised numerous oil globules arranged in two rows inside a chloroplast lobe, underlying the microtubules of the longitudinal microtubular root (LMR/r1) (Supplementary figs S5, S7).

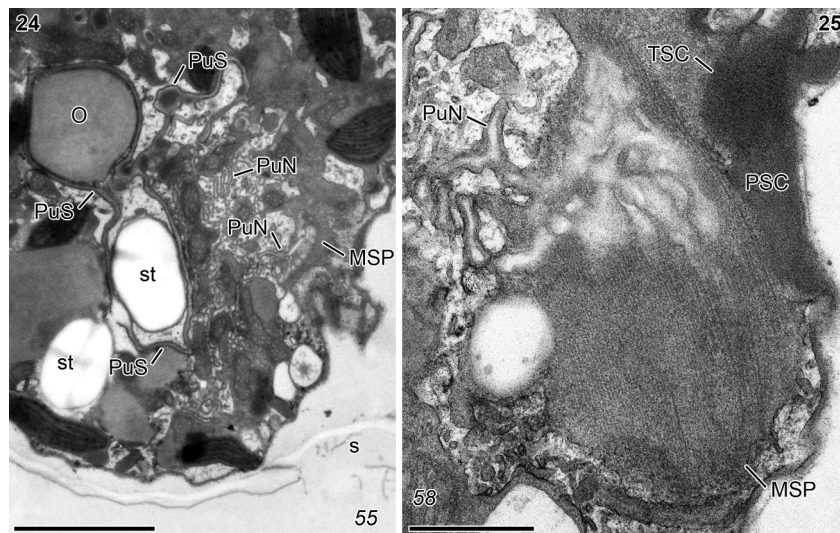
In oblique sections through the apical pore complex (apc) the apical cytoplasm appeared highly vesiculate (Supplementary fig. S12). Serial sections through the apc revealed both round and elongated vesicles underneath the pore, with some tubular vesicles extending through the apical-most cytoplasm toward the cover plate (Supplementary figs S8–S12). The cytoplasm inside the pore plate opening, underneath the cover plate, was lined with electron-opaque material, from which radiated several fibres that were striated in at least some views (Supplementary figs S8–S11).

Pusular system

The pusular system of the cells examined was rather extensive and complex. Three distinct portions are tentatively recognized based on the appearance and

distribution in the cell of the pusular elements (Supplementary figs S5, S12–S19, Figs 24, 25, 28–36). The most extensive portion was mainly composed of a flat, sheet-like vesicle that extended for nearly 4 μ m from the ventral area into the middle and right side of the cell. It occurred in a vesicle-rich cytoplasmic region that also contained starch grains and oil droplets (Supplementary figs S13, S17, Fig. 24). This so-called pusular sheet (PuS) was a flat vesicle with a somewhat electron-opaque lumen mostly 40–50 nm thick (Fig. 24). It attained its largest development near the mid-ventral area and extended anteriorly toward the cell's right, where it progressively lost its nearly uninterrupted flat appearance and ramified into tubular portions and smaller vesicles with different profiles (Fig. 24). In its posterior part, the pusular sheet ramified extensively into more irregular vesicles that contained numerous, somewhat elongated, electron-opaque bodies about 100 \times 400 nm (Supplementary figs S17, S19). Similar bodies occurred inside the more or less collapsed longitudinal flagellar canal (LFC), where some ramifications of the pusular sheet attached (not shown).

A different pusular arrangement accompanied the microtubular strand of the peduncle (MSP, described



Figs 24–25. *Parvodinium* strain from Buçaco, TEM. Ventral area with pusular system and microtubular strand of the peduncle (MSP); continuation of the series of sections shown in Supplementary figs S12–S16. Slanted numbers indicate the section number in the series. **Fig. 24.** The single row of microtubules from the microtubular strand of the peduncle and two pusular elements: the flat, sheet-like vesicle (PuS) and the network of pusular tubes (PuN). **Fig. 25.** Emergence area of the peduncle with the MSP extending along the PuN. The striated collar of the peduncle (PSC) contacts the transverse striated collar (TSC). O, oil droplets; s, sulcus; st, starch grains. Scale bars: **Fig. 24**, 2 μm ; **Fig. 25**, 500 nm.

below), extending from the area of emergence of the peduncle (Supplementary figs S12–S16, **Figs 24, 25, 28**; PuN). This pusular area was mainly composed of 20–30 nm wide tubes, which ramified and anastomosed, forming a roughly cylindrical network. The lumen of the tubes of this part of the pusule was distinctly more electron-translucent than that of the PuS (Supplementary figs S14, S16, **Figs 24, 25**). The orientation of the PuN was approximately parallel to the PuS and the two systems were perhaps connected by narrow tubes (**Fig. 24**); however, we were unable to demonstrate a continuity between membranes of the tubes and the sheet, possibly because of the convoluted shape of the tubes in the area between the two pusular systems. No pusular elements were visible in the emergent part of the peduncle (Supplementary fig. S6).

The third pusular arrangement comprised a single, somewhat flattened tube about 100×250 nm in cross section, which opened into the anterior-dorsal side of the transverse flagellar canal (TFC) and extended into the left-dorsal side of the cell (**Figs 31–36**, white arrow). Parts of the tube membrane had a dotted appearance similar to that visible in the upper tube of Supplementary fig. S19. The tube descended for about 2 μm and turned toward the centre of the cell, where it apparently branched (not shown); the branches approached the other portions of the pusule making their distinction uncertain, although the dotted appearance of some tubes in the ventral area may indicate their continuity with this transverse pusular tube.

Microtubular strand of the peduncle (MSP)

A single row of microtubules was found in the extruded portion of the peduncle and in the ventral area of the cell, near the basal bodies. This MSP extended into the cell, arching and breaking up into several groups of microtubules along its 15- μm path (Supplementary figs S12–S19, **Figs 24–30**). A schematic view of the whole path of the MSP is given in a left-ventral view in **Fig. 26**. The position of the MSP relative to the components of the flagellar apparatus is shown in left view in **Fig. 27**.

About 35 microtubules tightly arranged as a single row formed the MSP near the emergence area of the peduncle (**Figs 25–27**). A fibrous collar (striated collar of the peduncle, PSC) surrounded the cytoplasm, including the MSP, that extended from the cell (**Figs 25, 27**). In the ventral area the MSP passed along the network of pusular tubes, PuN (**Figs 24, 25**) and extended on the ventral-right side of the basal bodies (**Figs 26–30**) toward an accumulation body (ab) on the anterior-left area of the epicone (Supplementary figs S12–S16, **Fig. 26**). The path of the MSP between the ventral area and the anterior edge of the ab was somewhat wavy (Supplementary figs S12, S14, **Fig. 26**), with a tendency for the microtubules to separate irregularly into several groups that appeared to re-associate further along (not shown). Electron-opaque bodies were visible near most of the ventral portion of the MSP (Supplementary figs S15, S18).

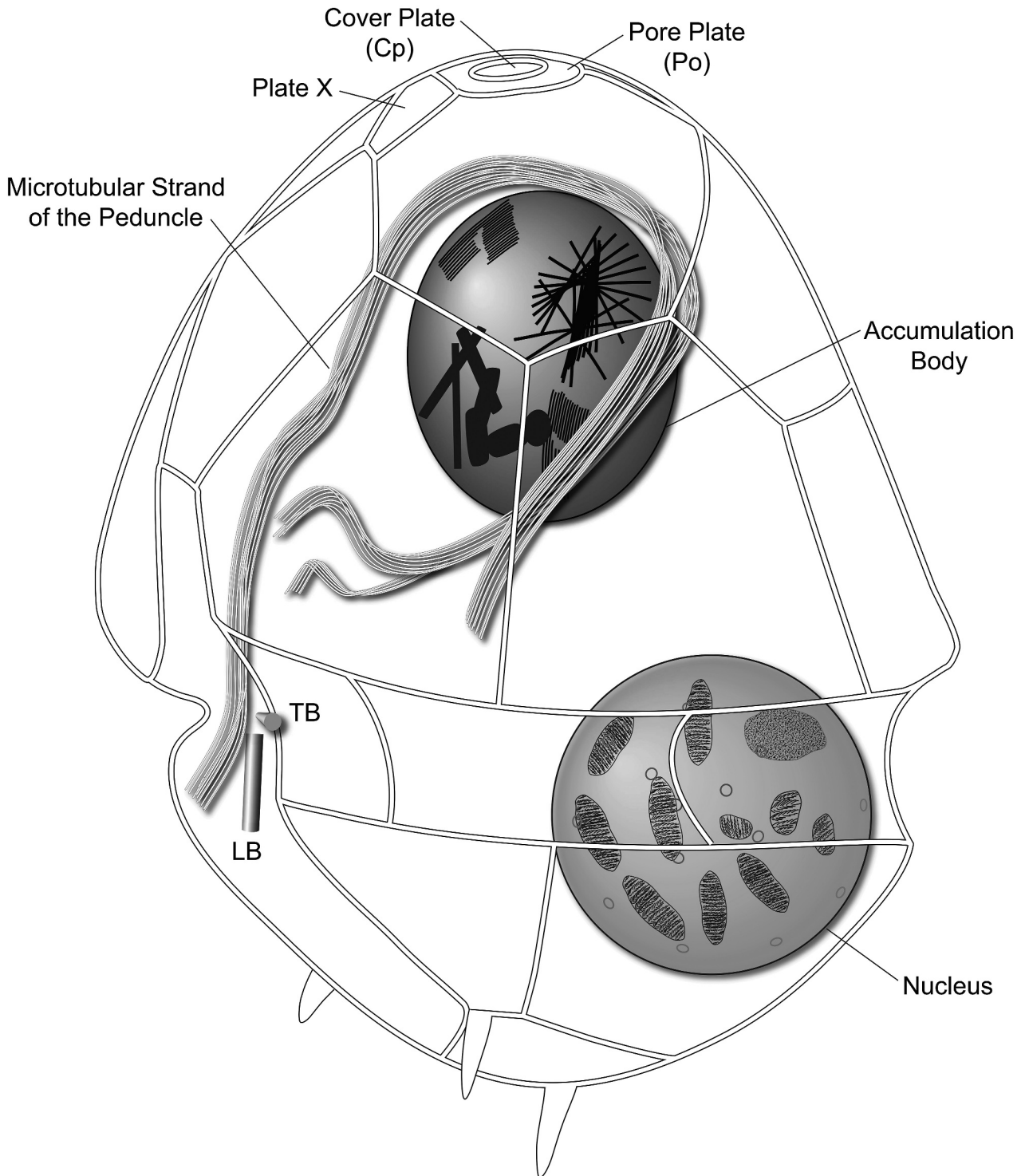


Fig. 26. Schematic representation of a cell's left-ventral view showing the plates and internally, the relative position of the nucleus, accumulation body, flagellar apparatus (represented by the basal bodies) and the path of the microtubular strand of the peduncle (MSP).

The MSP inflected to the left around the anterior-dorsal part of the ab and divided into two groups with slightly different routes (Supplementary figs S13, S15, S17, S18, Fig. 26). Both of these groups divided again creating a complex set of small microtubular strands, visible in sections through the mid-ventral part of the cell (Supplementary figs S15, S18, microtubular groups 1–4).

Flagellar apparatus

A schematic reconstruction of the flagellar apparatus as seen from the left of the cell is given in Fig. 27. Serial sections of the flagellar base area in an anterior-ventral-left point of view are shown in Figs 28–40; and from approximately left to right, with the cell slightly tilted toward the observer, in Figs 41–44. The basal bodies were

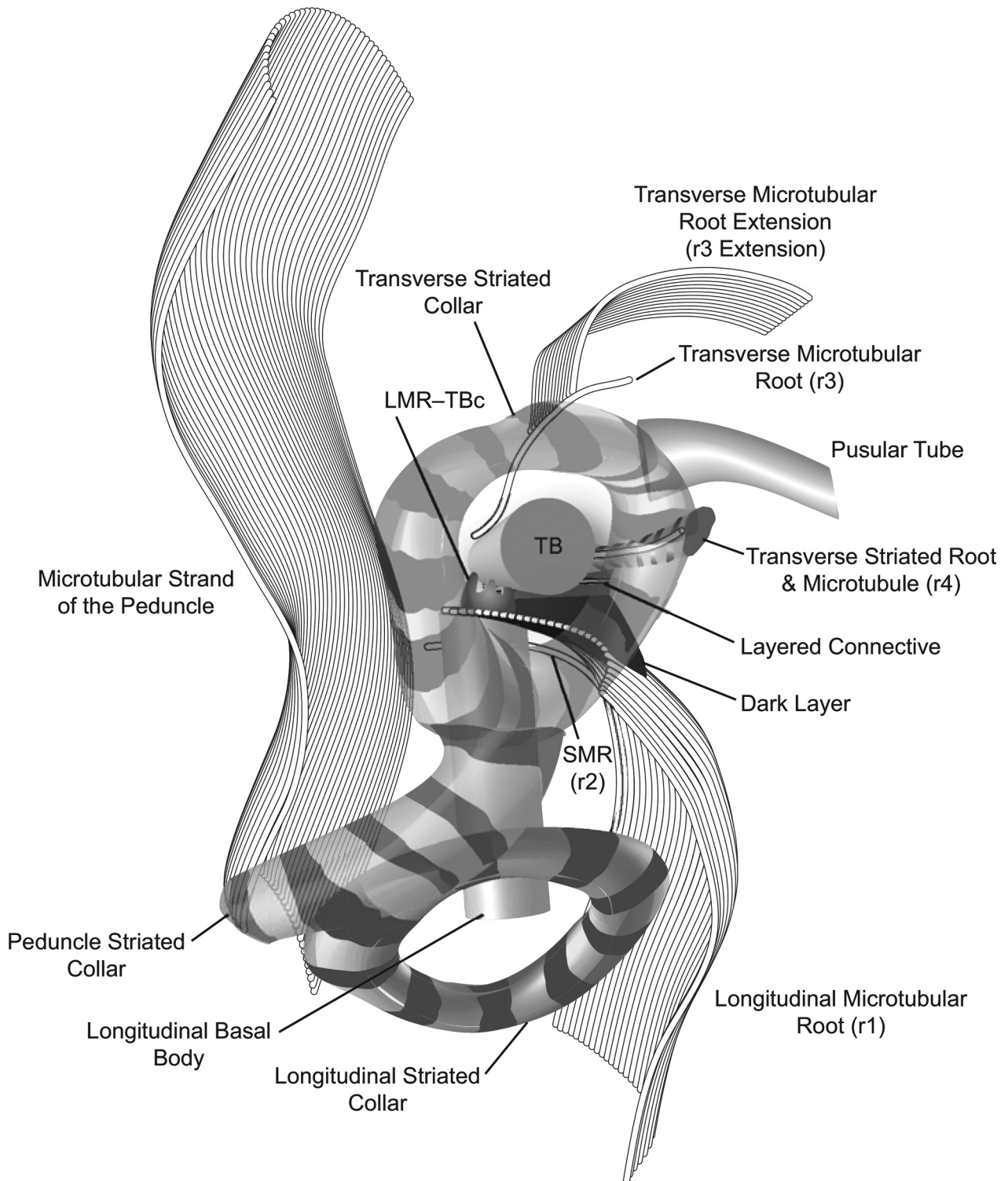
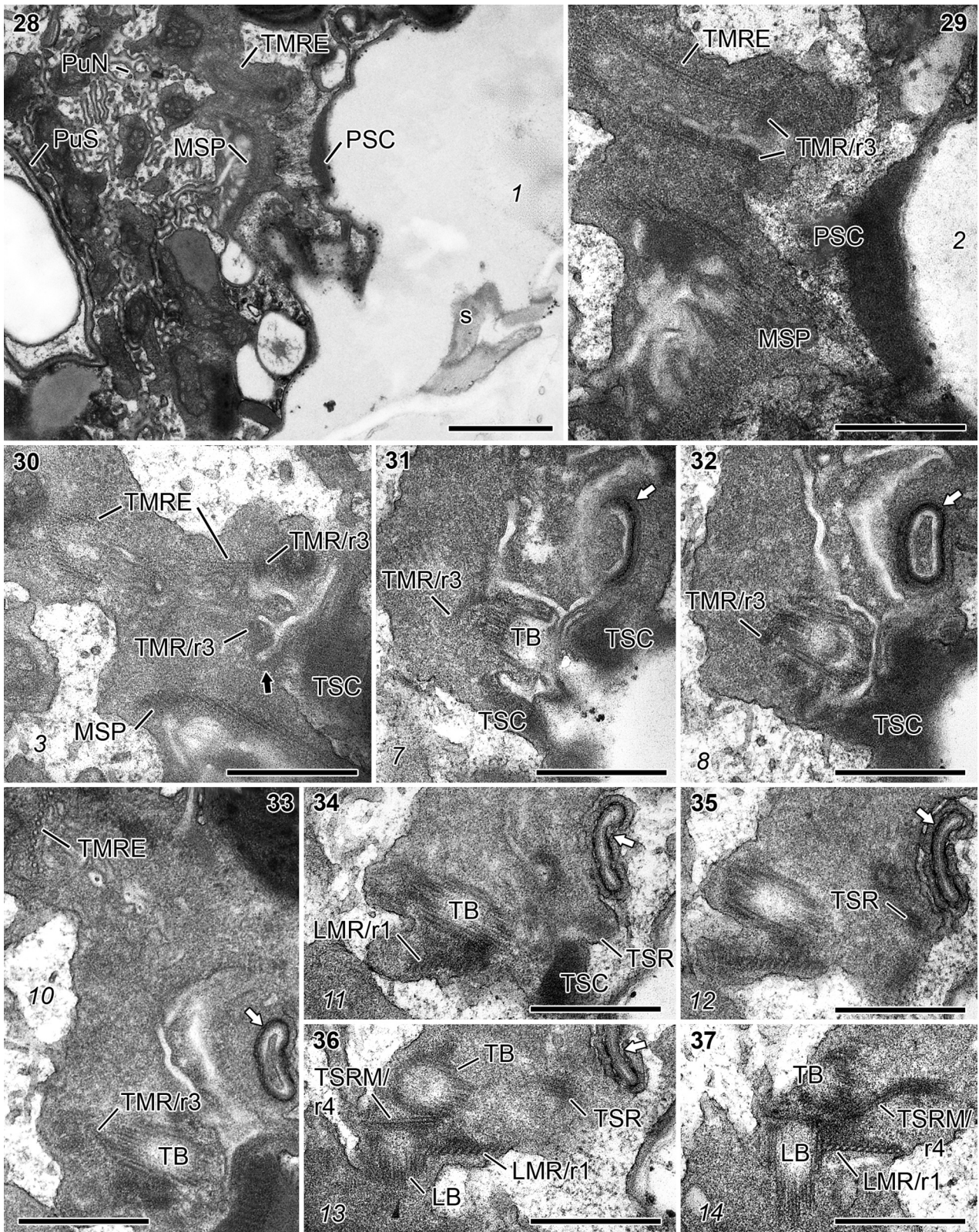


Fig. 27. Schematic representation of the flagellar base area of *Parvodinium*, viewed from the left side of the cell. The transverse and peduncle striated collars are made transparent to allow observation of underlying structures. SMR (r2), single-stranded microtubular root; LMR-TBc, three short fibrous connectives between the layer of electron-opaque material on the anterior-dorsal side of the LMR/r1 and microtubular triplets of the TB.

inserted at an angle of $\sim 90^\circ$, as estimated from serial sections (Figs 27, 31–44). Fibrous material was visible around the areas of emergence of each flagellum and the peduncle (marked as striated collars, TSC, LSC or PSC, in Figs 27–32, 34, 38–40, 43, 44). Two microtubular roots were associated with each basal body. A single

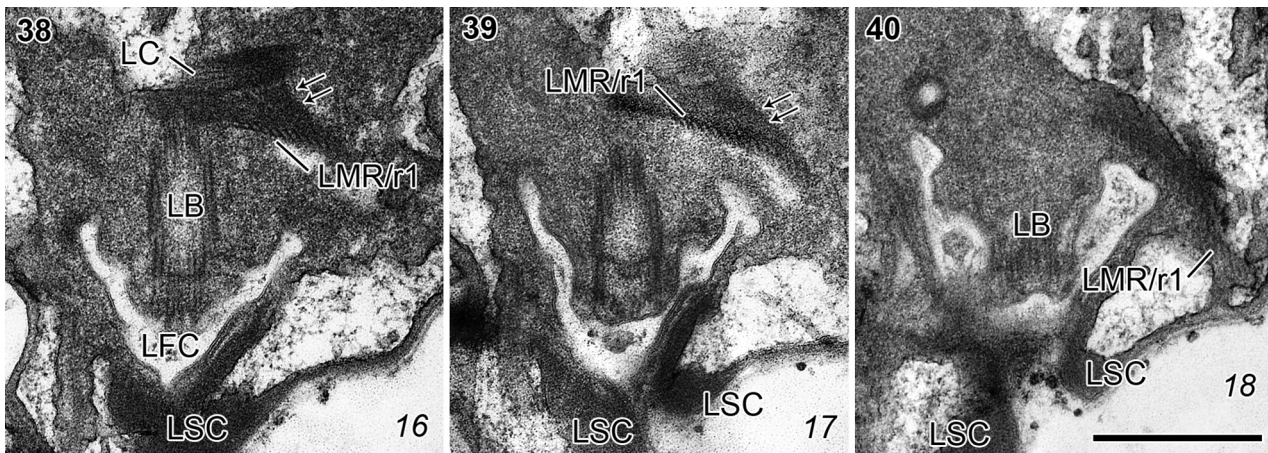
microtubule, forming the transverse microtubular root (TMR/r3), attached to the proximal-anterior end of the TB, extended towards the upper side of the transverse flagellar canal (TFC) and nucleated a strand of about 11 microtubules (the transverse microtubular root extension, TMRE/r3 extension) that curved around the



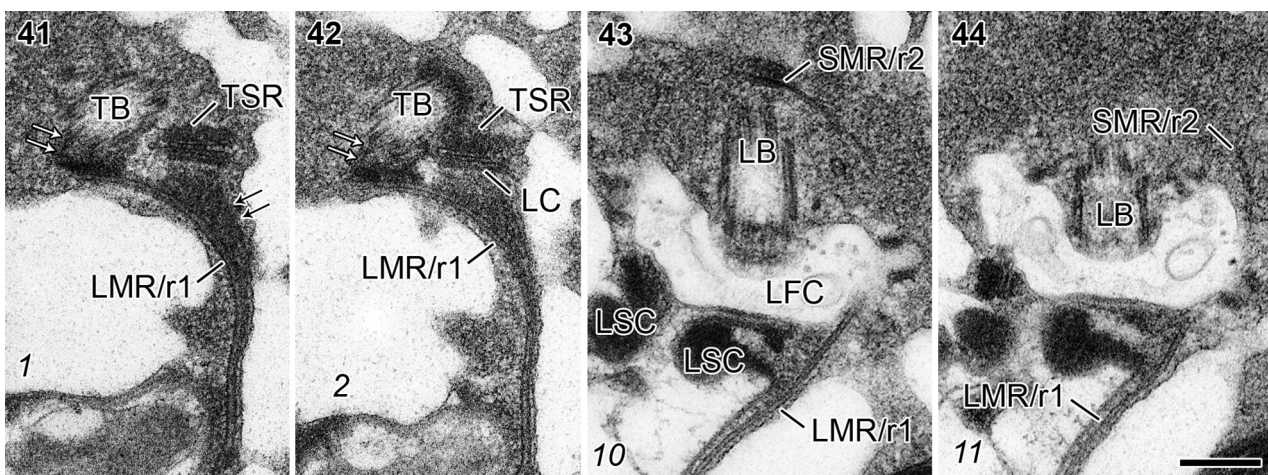
Figs 28–37. *Parvodinium* strain from Buçaco, flagellar apparatus, TEM. Non-adjacent serial sections progressing toward the left-dorsal side, seen from the right-ventral side. Slanted numbers indicate the section number in the series. **Fig. 28.** Ventral area of the cell, somewhat detached from the theca, with the pusular system (PuN and PuS), the microtubular strand of the peduncle (MSP) and the transverse microtubular root extension (TMRE). **Figs 29, 30.** The TMRE and the MSP are present near the peduncle striated collar (PSC) and the transverse striated collar (TSC). The TMRE is nucleated by the transverse microtubular root (TMR/r3), that runs near collared pits (black arrow). **Figs 31–33.** The proximal end of the TMR/r3 approaches the proximal end of the transverse basal body (TB). A flattened pusular tube (white arrow) opens into the anterior-dorsal side of the transverse flagellar canal. **Figs 34–37.** The proximal end of the longitudinal microtubular root (LMR/r1) is visible contacting the proximal end of the longitudinal basal body (LB). The transverse striated root (TSR) and its associated microtubule (TSRM/r4) extend from near the TSC to the proximal-dorsal side of the TB. Scale bars: Fig. 28, 1 µm; Figs 29–37, 500 nm.

anterior margin of TFC and continued in a posterior-left direction (Figs 27–33). The transverse striated root and its associated microtubule (TSR and TSRM/r4) progressed from the proximal-dorsal side of the TB toward the transverse striated collar (TSC; Figs 27, 34–37, 41, 42). Both TSR and TB contacted the anterior part of a layered connective (LC) about 250 nm long and 70 nm thick (Figs 27, 38, 41, 42). A layer of electron-opaque material connected the posterior layer of the LC to the dorsal side of the longitudinal microtubular root (LMR/r1) (Figs 27, 38, 39, 41). Three short fibrous connectives extended from microtubular triplets of the TB to a layer of electron-opaque material on the dorsal face of the proximal end of the LMR/r1

(Figs 27, 41, 42, double white arrow). About 10 microtubules were present in this proximal end of the LMR/r1, but this number increased towards the sulcus (Figs 36–40). The right-hand side of the LMR/r1 contacted the proximal end of the LB (Figs 27, 36–44). The distal part of the LMR/r1 extended posteriorly on the left side of the longitudinal flagellar canal (LFC), passed next to the LSC and continued along the ventral side, adjacent to the amphiesmal vesicles lining the sulcus. A single-stranded microtubular root (SMR/r2) extended from the proximal-right side of the LB for about 650 nm, in a path nearly parallel to the LMR/r1 and ended near the surface of the LFC (Figs 27, 43, 44).



Figs 38–40. *Parvodinium* strain from Buçaco, flagellar apparatus, TEM. Continuation of the series of sections shown in Figs 28–37; adjacent serial sections. Slanted numbers indicate the section number in the series. The layered connective (LC) is linked, in its posterior side, to a layer of electron-opaque material (double arrows) that covers the dorsal side of the longitudinal microtubular root (LMR/r1). The longitudinal striated collar (LSC) surrounds, almost completely, the opening of the longitudinal flagellar canal (LFC). LB, longitudinal basal body. Scale bar: Figs 38–40 to the same scale, 500 nm.



Figs 41–44. *Parvodinium* strain from Denmark, flagellar apparatus, TEM. Non-adjacent serial sections progressing toward the right-antapical side, seen from the left-apical side. Slanted numbers indicate the section number in the series. **Figs 41, 42.** Three short fibres (double white arrows) connect the transverse basal body (TB) to the dorsal side of the proximal end of the longitudinal microtubular root (LMR/r1). Note the layer of electron-opaque material (double black arrows) that covers the dorsal side of the LMR/r1. **Figs 43, 44.** The single-stranded microtubular root (SMR/r2) is visible on the right side of the longitudinal basal body (LB). LC, layered connective; LFC, longitudinal flagellar canal; LSC, longitudinal striated collar; TSR, transverse striated root. Scale bar: Figs 41–44 to the same scale, 200 nm.

Phylogeny

The position of *Parvodinium* within a large assemblage of dinoflagellates was examined by phylogenetic analyses based on nuclear-encoded partial LSU rDNA sequences (a single-gene tree). The resulting tree topology is shown in Fig. 45 and here *Parvodinium* formed a monophyletic group (marked as *Parvodinium* spp.). However, this only received little support from posterior probability (PP = 0.83) and Maximum likelihood bootstrap (BS = 59%). This clade containing species of *Parvodinium* was divided into two lineages, each fairly well supported. Hence, one clade comprised *Parvodinium mixtum* Kretschmann, Owsiany, Zerdoner & Gottschling, *P. parvulum* (Wołoszyńska) Na Wang, K.N.Mertens, H.Gu, *P. elpatiewskyi*, *Parvodinium* 'Buçaco', '*Peridinium inconspicuum*' strains CCAP 1140 and UTEX 2255 (PP = 0.97 and BS = 94%). The other clade contained '*Peridinium umbonatum* var. *inaequale*', *Parvodinium* cf. *centenniale*, *Parvodinium* cf. *umbonatum* strain GeoM*795 and *Peridinium centenniale* (Playfair) Carty (PP = 0.94 and BS = 79%). The clade, marked as *Parvodinium* spp., formed a sister group to *Johsia chumphonensis* Z.Luo, Na Wang, K.N.Mertens & H.Gu, *Peridiniopsis borgei* Lemmermann and *Palatinus* spp. However, this branching pattern received very little support from posterior probability (PP = 0.71) and no support from ML bootstrap (BS < 50%). The larger clade was part of a polytomy containing seven other lineages. The deepest lineages forming the backbone of the tree containing dinoflagellates were also unresolved (polytomy). However, most of these individual lineages received high branch support from posterior probabilities and bootstrap replicates.

The phylogenetic inference based on the concatenated data matrix and containing species closely related to *Parvodinium* based on the analysis of LSU rDNA revealed fairly good to moderate support for a monophyletic origin of *Parvodinium* from posterior probability and bootstrap, respectively (PP = 0.95 and BS = 70%) (Supplementary fig. S20). The seven species (nine strains) assigned to *Parvodinium*, and the clade comprising *Palatinus apiculatus* (Ehrenberg) Craveiro, Calado, Daugbjerg & Moestrup, *Peridiniopsis borgei* and *Johsia chumphonensis* formed a highly supported monophyletic clade (PP = 1.0 and BS = 98%). For the core group of *Parvodinium* species, a highly supported relationship was observed between the three strains of *P. mixtum* but also for the shared, and based on the short branch lengths, a relative recent ancestry between *P. parvulum*, *P. elpatiewskyi*, *P. trawinskii*

Kretschmann, Owsiany, Zerdoner & Gottschling, *Parvodinium* 'Buçaco' and *P. mixtum* (PP = 1.0 and BS = 100%). The other deep lineage of ingroup taxa formed a highly supported lineage comprising *Pfiesteria*, *Apocalathium*, *Scrippsiella* spp., *Naiadinium*, *Duboscquodinium* and *Theleodinium* (PP = 1.0, BS = 100%). Note that *Scrippsiella* did not form a monophyletic group due to the clustering of *Duboscquodinium collinii*.

Discussion

Identity and phylogenetic affinities of the Buçaco strain

The cells of the culture strain examined showed the general features of the *P. umbonatum*–*P. inconspicuum* species complex. Relevant characters include the conspicuous apical pore complex located at the centre of the cell apex, the two similar-sized anterior intercalary plates symmetrically positioned on the dorsal side of the epitheca, the slightly descending cingulum, delimiting the longer anterior part of the cell from the shorter hypotheca, and the moderately compressed, ovoid to ellipsoid shape of the cell. Particularly significant is the shape of the sulcus, forming a trapezoid indentation in the epitheca and strongly widening toward the antapex. All the characters mentioned above are present in *P. mixtum*, *P. trawinskii* and *P. marciniakii* Kretschmann, Owsiany, Zerdoner & Gottschling (Kretschmann *et al.*, 2018), all of which appear in the same well-supported clade of the concatenated phylogenetic tree (Supplementary fig. S20) as *Parvodinium* 'Buçaco'. The other species in that clade, *P. elpatiewskyi*, lacks the intercalary plates but its sulcus shows the same general outline, slightly indenting the epitheca and widening toward the antapex (Moestrup & Calado, 2018; Kretschmann *et al.*, 2019). *Parvodinium* from Buçaco appears as a sister taxon to *Parvodinium mixtum* (Supplementary fig. S20), with which it shares the same pattern of plate overlap (Kretschmann *et al.*, 2018).

The original description of *Peridinium inconspicuum* Lemmermann was rather brief, did not include any details about the plates and was not accompanied by an illustration (Lemmermann, 1899). The earliest illustrations by Lemmermann show the oval outline of the cell, the slightly descending cingulum, the axial position of the apical pore and the presence of three spines aligned with the sutures of the antapical plates (Lemmermann, 1905, 1910; figures reproduced in Moestrup & Calado, 2018). Although Lemmermann's (1910) figures lack precision, as seen in the representation of a similar-looking narrow plate at the apex in both ventral and dorsal views, the position of the three spines in a dorsal view of the

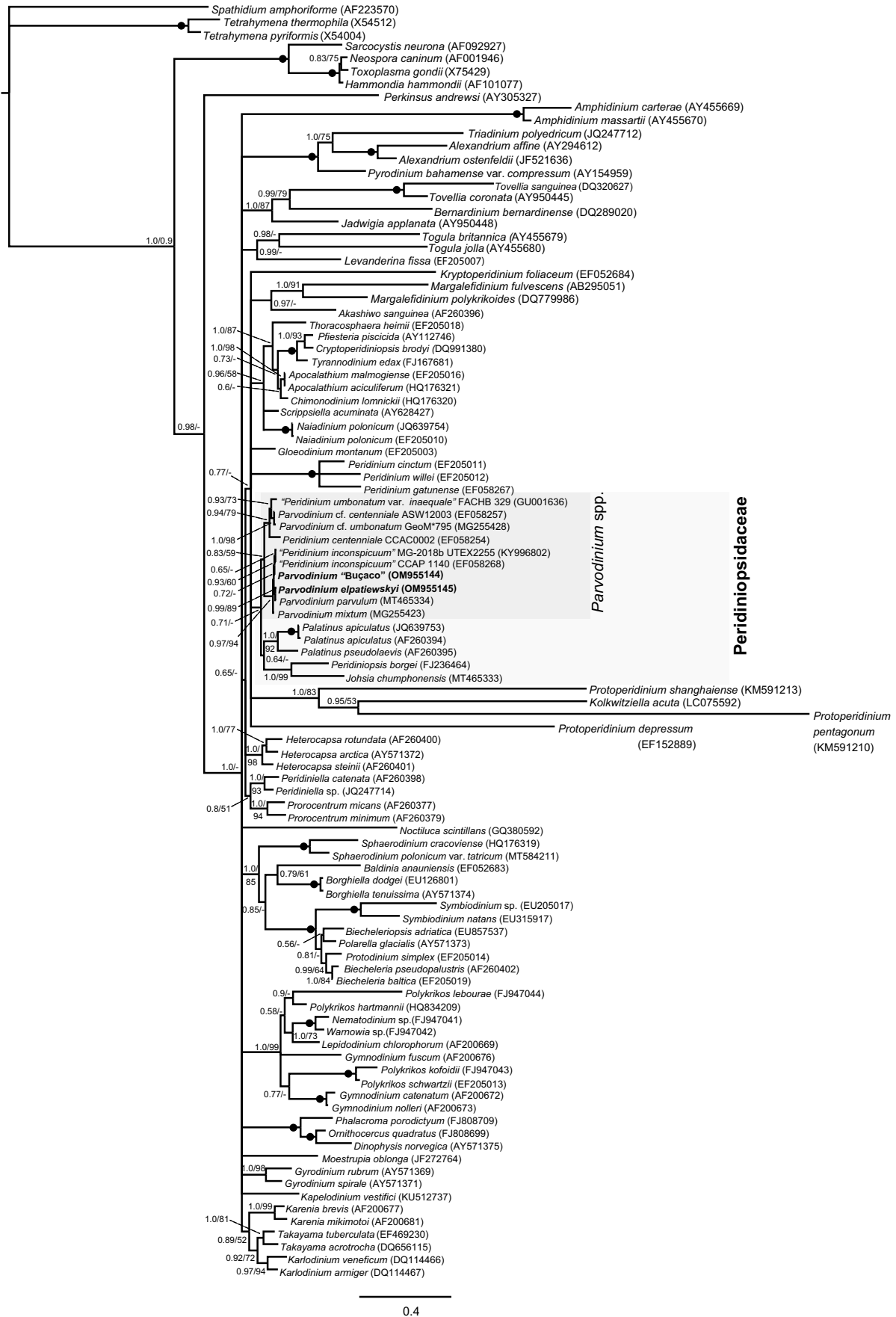


Fig. 45. Phylogeny based on partial nuclear-encoded LSU rDNA sequences (1667 bp including introduced gaps) of 54 genera of dinoflagellates and inferred from Bayesian analysis. For this analysis three ciliates, four apicomplexans and *Perkinsus andrewsi* were used as outgroup taxa. Branch support was evaluated from posterior probabilities (PP ≥ 0.5) from Bayesian analyses and bootstrap (1000 replications, BS $\geq 50\%$) from maximum likelihood analyses, respectively. These support values are written to the left of internodes. A hyphen (-) indicates values below 0.5 for PP and 50% for bootstrap. GenBank accession numbers and, in some cases, strain numbers for *Parvodium* spp. are written after the species epithet. The evolutionary lineage containing *Parvodium* spp. is marked in grey, and the sequences determined in this study are in bold. The branch lengths are proportional to the number of character changes, see scale bar below the phylogenetic tree.

cell (Lemmermann, 1910, p. 663, fig. 29), and the distinctly smaller size of antapical plate 1, suggest the arrangement we document for the Buçaco strain.

Stein's (1883) original drawings of *Peridinium umbonatum* show details of the main plates in ventral and dorsal views, and include the complete tabulation of the epitheca in an apical view that shows a very slight dorsoventral compression. The cell outline appears distinctive in Stein's drawings, but the rather long, nearly truncated-cone-shaped ring of precingular plates has not been documented from other specimens. A description of *P. umbonatum* was included in Lemmermann (1910), who added to two of Stein's illustrations, in ventral and dorsal view, an apical and an antapical view by Schilling (1891), both of which showed a distinct dorsoventral compression. Lefèvre (1932) summarized the observations on *P. umbonatum*, *P. inconspicuum* and their infraspecific taxa, and established the concepts for these taxa that would influence the application of the names for the following decades (Schiller, 1935; Huber-Pestalozzi, 1950; Starmach, 1974). The overlap of features recognized by Lefèvre (1932) for the two species is quite extensive, with only size as a guide to identify populations of small cells (15–25 µm long) as *P. inconspicuum* and populations of cells longer than 30 µm as *P. umbonatum*, and leaving an uncomfortable overlap in the 25–30 µm range. In view of the natural variability in cell size found in many populations, and of the difficulty of selecting features that could reliably distinguish *P. inconspicuum* from *P. umbonatum*, the decision to treat the two names as synonyms was understandable (Popovský & Pfister, 1986, 1990). However, the description of new taxa by the combined application of morphological and genetic analyses demonstrated more species-level diversity than previously recognized and highlighted the need for well-defined (morphologically and genetically) taxonomic and nomenclatural reference points in this group of species (Kretschmann *et al.*, 2018). The description of new taxa in this core group of *Parvodinium* species presupposes the establishment of a distinction between the newly described species and these older names. Several GenBank entries with the names *P. inconspicuum* and *P. umbonatum* are available and these names have been included in published phylogenetic trees (Logares *et al.*, 2007; Kretschmann *et al.*, 2018; Luo *et al.*, 2019). However, the morphological characterization of the strains from which the DNA sequences were determined is scarce or non-existent and the topological location of strains with the same name in phylogenetic trees is often inconsistent (Saldarriaga *et al.*, 2001; Stern *et al.*, 2012; Kretschmann *et al.*, 2018). Nomenclatural stability will eventually require that a strain be accepted as fixing the application of each

name. While the choice of a reference strain for each of the species *P. umbonatum* and *P. inconspicuum* may have to be largely arbitrary, given the difficulty of defining characters and distinguishing the species morphologically, it is desirable that the selection of a reference strain be accompanied by a detailed morphological analysis and include the sequencing of, at least, major portions of the ribosomal operon, which are commonly used for phylogenetic inferences in dinoflagellates. A strain with small cells and a morphology compatible with early drawings of the species, similar to the Buçaco strain described herein, would appear eligible as a reference point fixing the application of the name *P. inconspicuum*. Ideally, the selected strain would come from one of the original locations for the taxon, namely two islands in Hawaii (Molokai and Oahu) and Chatham Islands, off the coast of New Zealand, some 7500 km south of Hawaii.

The selection of a morphologically and genetically characterized strain for fixing the application of the name *P. umbonatum* may have a larger impact on nomenclature because this is the type species of the genus. The use of the name in published phylogenetic trees may induce the tacit selection of one of the sequences available in GenBank as representing the phylogenetic position of *P. umbonatum*. However, the retrieval of two fairly well supported, separate lineages with *Parvodinium* species in the phylogenetic tree based on LSU rDNA (Fig. 45) recommends a closer look at the taxa in the clade containing *Parvodinium cf. umbonatum* GeoM*795, '*Peridinium umbonatum* var. *inaequale*' and *P. centenniale*. For example, EF058254 is currently labelled 'Dinophyceae sp. strain CCAC0002' in GenBank; it was submitted as '*Peridinium centenniale* CCAC0002' by Logares *et al.* (2007) and was referred as *Parvodinium centenniale* by Kretschmann *et al.* (2018). Both *Parvodinium cf. umbonatum* GeoM*795 and '*Peridinium umbonatum* var. *inaequale*' were illustrated, and they both show a broadly round epitheca that is wider than the hypotheca (Zhang *et al.*, 2011; Kretschmann *et al.*, 2018). A distinctly narrower hypotheca was the basis for the original distinction of *Peridinium umbonatum* var. *inaequale* Lemmermann (1910, pp. 669, 670), which, however, still showed the pronounced widening of the sulcus toward the antapex. In his monograph, Lefèvre (1932, pp. 123, 124) adopted a broader concept of the variety and combined illustrations of cells with the typical widening sulcus and a symmetrical tabulation with others showing a smaller sulcus with a round posterior end, an off-axis apical pore and a somewhat asymmetrical arrangement of plates on the epitheca – a combination of characters reminiscent of *P. centenniale* as depicted by Playfair (1920) and Ling *et al.* (1989). The illustrations given for

Parvodinium cf. *umbonatum* GeoM*795 show a narrower sulcus that closes posteriorly on the ventral side, and a slight asymmetry of outline and plate disposition, which suggest affinity with *P. centenniale* (Kretschmann *et al.*, 2018). Since the original illustrations of *P. umbonatum* show a symmetrical epithecal tabulation and the posteriorly widening sulcus, the effect of selecting a reference strain for the type of *Parvodinium* from this clade with apparent affinities with *P. centenniale* would be to change the application of the name relative to the one that prevailed for more than eight decades, viz. a species closely related to, and difficult to distinguish from, *P. inconspicuum*. Since no DNA sequence can be assigned at present to a strain unequivocally with the morphology of *P. umbonatum*, we suggest that stability and historical continuity of the application of species names in *Parvodinium* may be achieved by selecting as reference strain a population, or culture, with the general features of species in the clade of *P. inconspicuum*, *P. mixtum* and *P. trawinskii*, and an average cell length near or above 30 µm.

General ultrastructure and apical pore complex

Cells of the *Parvodinium* strain from Buçaco showed the fine-structural features typical of a photosynthetic dinoflagellate: a nucleus with condensed chromosomes, numerous chloroplast profiles, pusular system, trichocysts, and starch grains and oil droplets as reserves. No pyrenoids were observed; however, the chloroplast lobes had a radial disposition towards the centre of the cell compatible with what was observed by Seo & Fritz (2002) in '*Parvodinium inconspicuum*' strain UTEX LB2255, which appears in our LSU rDNA-based phylogenetic tree in the same clade as *Parvodinium* from Buçaco (accession KY996802). The quantity of starch accumulated and the presence or absence of a central pyrenoid (expressed as thylakoid-free areas of chloroplast lobes) were reported by Seo & Fritz (2002) to vary according to the light or dark phase in cultures of some dinoflagellates. This variability was not examined in our strain and, although it cannot be excluded that a central region rich in chloroplast lobes with thylakoid-free areas resembling a central compound pyrenoid may be formed in some conditions, no traces of a well-defined, central pyrenoid were found. The presence of a more or less complex central pyrenoid has been considered characteristic of other members of the Peridiniopsidaceae (Gottschling *et al.*, 2017). *Peridiniopsis* and *Johsia* have a single round pyrenoid surrounded by starch, whereas the central pyrenoid in *Palatinus* radiates into the associated chloroplast lobes (Calado & Moestrup, 2002; Craveiro *et al.*, 2009; Luo *et al.*, 2020). In contrast,

typical Peridiniaceae, e.g. *Peridinium cinctum* (O.F. Müller) Ehrenberg and *P. gatunense* Nygaard, do not show this type of large, well-defined pyrenoid, only thylakoid-free areas in some chloroplast lobes (Messer & Ben-Shaul, 1969; Calado *et al.*, 1999).

An eyespot type A (Moestrup & Calado, 2018), consisting of one or more rows of lipid globules included in a chloroplast lobe, was observed in our strain and agrees with observations from Luo *et al.* (2020) for *Parvodinium parvulum*. An eyespot of type A is also present in *Palatinus* (Craveiro *et al.*, 2009) and '*Scrippsiella*' *hexapraecingula* (Horiguchi *et al.*, 1999), whereas an eyespot of type B, with a layer of crystal-containing vesicles overlying a lipid globule-containing chloroplast lobe, was found in *Peridiniopsis borgei* and in *Johsia chumphonensis* (Calado & Moestrup, 2002; Luo *et al.*, 2020). The eyespot type A is most common in the Peridinales and Thoracosphaerales, while the eyespot type B has been mainly found in the family Borghiellaceae (Moestrup & Calado, 2018).

An apical pore complex is present in almost all peridinioids but is absent from species of *Peridinium* subg. *Cleistoperidinium* (Peridiniaceae) and from *Palatinus*, the only genus of the Peridiniopsidaceae without it. When present, the apical pore is usually underlain by fibres (apical fibrous complex) above a cytoplasm region rich in vesicles (e.g. Roberts *et al.*, 1987; Hansen *et al.*, 1996; Craveiro *et al.*, 2011). The appearance of the fibrous complex is somewhat influenced by the type of fixation (Calado & Moestrup, 2002), which complicates comparisons between different taxa. Our observations on the *Parvodinium* strain from Buçaco are compatible with what was shown in cells of *Scrippsiella sweeneyae* Balech, *Peridiniopsis borgei*, *Chimonodinium lomnickii* (Wołoszyńska) Craveiro, Calado, Daugbjerg, Gert Hansen & Moestrup and *Theleodinium calcisporum* Craveiro, Pandeirada, Daugbjerg, Moestrup & Calado, all of which were fixed with a mixture of glutaraldehyde and osmium tetroxide: an uninterrupted fibrous layer lining the inner cylindrical raised area of the pore plate, which extends posteriorly along the cell surface as several independent fibres (Roberts *et al.*, 1987; Calado & Moestrup, 2002; Craveiro *et al.*, 2011, 2013).

Pusular system

The complex pusular system found in *Parvodinium*, with three distinct areas, has not been previously described from other dinoflagellates. The so-called pusular network (PuN) resembles, to some extent, the flattened and ramified pusular vesicles of *Scrippsiella trochoidea* (F.Stein) A.R.Loeblich (Thoracosphaerales), which however, was restricted to a smaller region on the right mid-ventral side of

the cell (Craveiro *et al.*, 2011). Pusular structure was described in detail in two other Peridiniopsidaceae, *Peridiniopsis borgei* and *Palatinus apiculatus*; both showed a large sac pusule connected to the LFC (Calado & Moestrup, 2002; Craveiro *et al.*, 2009). A sac pusule was not observed in the *Parvodinium* cells examined, either because the collapse of the ventral region may have concealed this feature, or because it is absent from this species. Both *Peridiniopsis borgei* and *Palatinus apiculatus* have flattened pusular vesicles scattered in the cell; in addition, two distinct pusular tubes connect to the TFC, and one to the LFC, of *P. apiculatus* (Calado & Moestrup, 2002; Craveiro *et al.*, 2009). A somewhat flattened pusular tube was also connected to the TFC in *Parvodinium*. Pusular tubes are some of the most common types of pusular structures in dinoflagellates, although they vary in number, width and in connecting to either the TFC or the LFC. The different pusular structures observed in *Parvodinium* contrast with the pusular organization of several other peridinioids, e.g. the genera *Chimonodinium* and *Apocalathium* (Thoracosphaeraceae), in which well-defined pusular tubes opening at the flagellar canals were the only pusular structures observed (Craveiro *et al.*, 2011, 2016).

Microtubular strand of the peduncle (MSP)

The MSP described herein for *Parvodinium* has a path inside the cell reminiscent of the one observed in *P. borgei* (Calado & Moestrup, 1997), although with a smaller number of microtubules (ca. 40 instead of ca. 80 in *P. borgei*). In both species the MSP extended from an extruded peduncle on the ventral area and was accompanied in this ventral region by electron-opaque bodies. The MSP continued toward the anterior-left side of the epicone in both *Parvodinium* and *P. borgei*, and in both cases the microtubular strand divided into several groups and was somewhat wavy in parts of its path (Calado & Moestrup, 1997). In contrast, *Palatinus* has a more simple strand of microtubules that lacks accompanying vesicles and does not extend into a peduncle; however, judging from its position and orientation it was considered homologous to the MSP (Craveiro *et al.*, 2009). The ultrastructure of the recently described marine genus *Johsia* was not examined in detail and no information concerning a MB or MSP is available (Luo *et al.*, 2020). ‘*Scrippsiella*’ *hexapraecingula* was observed with an extruded peduncle similar to those known to be supported by an internal MSP or MB; this is compatible with its phylogenetic relationship to *P. borgei* (Horiguchi & Chihara, 1983; Luo *et al.*, 2020). As a contrast to what has been observed in members of the Peridiniopsidaceae, in the Peridiniaceae, as represented by the type species

Peridinium cinctum, no type of microtubular system homologous to an MSP has been found (Calado *et al.*, 1999).

Flagellar apparatus

The general organization of the flagellar apparatus of peridinioids shows several variations concerning the presence or absence of small connectives linking its various components. One of these connectives, consisting of well-defined fibres associating the anterior-dorsal side of the LMR/r1 with two or three triplets of the TB (the LMR-TBc), was found in all members of the Peridiniopsidaceae for which detailed ultrastructural information is available: *Peridiniopsis borgei* (Calado & Moestrup, 1997), *Palatinus apiculatus* (Craveiro *et al.*, 2009) and *Parvodinium* (present work). In contrast to what was found in the Peridiniopsidaceae, the Thoracosphaeraceae revealed more variation, with some members also showing fibres attaching to two or three triplets of the TB (e.g. *Theleodinium calcisporum* and *Apocalathium aciculiferum* (Lemmermann) Craveiro, Daugbjerg, Moestrup & Calado; Craveiro *et al.*, 2013, 2016), whereas others, like *Chimonodinium lomnickii*, have a single, wider band of thin fibres attaching to the TB (Craveiro *et al.*, 2011). A third variation was found in *Naiadinium polonicum*, in which the basal bodies were more widely separated and the only fibrous connection between LMR/r1 and TB was provided by the LC (Craveiro *et al.*, 2015). In *Peridinium cinctum* (Peridiniaceae) the LC was also the only structure found linking LMR/r1 and TB (Calado *et al.*, 1999).

Within peridinioids, variation was also found in the arrangement and number of microtubules that form the extension of the TMR/r3. In the Peridiniopsidaceae, three different types of TMR/r3 extension were observed until now, the simplest being the one described here for *Parvodinium* with a single strand of 11 microtubules. In *Palatinus apiculatus* the TMR/r3 looped around the transverse flagellar canal before nucleating one or two rows of 20 microtubules (Craveiro *et al.*, 2009). A more peculiar TMR/r3 extension was described from *Peridiniopsis borgei*; it was composed of ca. 35 microtubules, of which 23 gradually assumed a cylindrical arrangement surrounding a fibrous core and extended around a large, central vesicle (Calado & Moestrup, 2002). In the Thoracosphaeraceae, *Chimonodinium lomnickii* also showed a TMR/r3 extension with an association with fibrous material, although it did not develop into the association seen in *P. borgei* (Craveiro *et al.*, 2011). These variations on the type of TMR/r3 extension, which cross family borders, seem to devalue its potential to reflect phylogenetic relationships.

A description of the fine structure of the family Peridiniopsidaceae, based on current knowledge, may be (see also Supplementary table S2): cells with an extensive network of chloroplast lobes bounded by three membranes, with thylakoids predominantly associated in lamellae of three (peridinin chloroplast type); thylakoid-free areas usually present in some chloroplast lobes; a large, inner pyrenoid, extending into radial lobes (*Palatinus*), round and surrounded by starch (*Peridiniopsis*, *Johsia*, ‘*Scrippsiella*’ *hexapraeicingula*), or pyrenoid absent (*Parvodinium*). Cytoplasmic channels sometimes penetrating the pyrenoid (*Palatinus*). Food reserves as starch grains and oil droplets, sometimes localized in different areas of the cell (*Peridiniopsis*). Eyespot present, of type A (*Parvodinium*, *Palatinus*, ‘*Scrippsiella*’ *hexapraeicingula*) or B (*Peridiniopsis*, *Johsia*) with at least two (*Parvodinium*, *Palatinus*, *Johsia*, ‘*Scrippsiella*’ *hexapraeicingula*) and up to six layers (*Peridiniopsis*; four layers in *Parvodinium parvulum*) of globules inside chloroplast lobe. Trichocysts present throughout the cell, of a single type. Apical pore complex present (*Peridiniopsis*, *Parvodinium*, *Johsia*, ‘*Scrippsiella*’ *hexapraeicingula*) underlain by apical fibrous complex (unknown in *Johsia* and ‘*Scrippsiella*’ *hexapraeicingula*), or absent (*Palatinus*). Mid-ventral area with extruded peduncle (*Peridiniopsis*, *Parvodinium*, ‘*Scrippsiella*’ *hexapraeicingula*) or peduncle absent (*Palatinus*; unknown in *Johsia*); microtubular strand homologous with MSP present (unknown in *Johsia*), reduced and without connection to the cell surface (*Palatinus*) or penetrating the peduncle and extending over the anterior area of the epicone and returning to the ventral area as separate rows of microtubules (*Peridiniopsis*, *Parvodinium*). Pusule (unknown in *Johsia* and ‘*Scrippsiella*’ *hexapraeicingula*) comprising flat vesicles and cylindroid tubes of variable diameter (*Palatinus*), a combination of rounded and flat vesicles (*Peridiniopsis*) or a very extensive assortment of ramifying flat and tubular vesicles with variable appearance (*Parvodinium*). Large sac pusule connected to the LFC (*Peridiniopsis*, *Palatinus*) or absent (*Parvodinium*). Flagellar apparatus (unknown in *Johsia* and ‘*Scrippsiella*’ *hexapraeicingula*) with basal bodies inserted about 100 nm apart and forming a 80–90° angle, each basal body associated with two microtubule-containing roots; LMR/r1 proximal end with 5–10 microtubules that do not extend beyond the LB, up to 30–40 microtubules distally; fibrous layer on dorsal face of LMR/r1 connecting to base of TB and TSR by an LC (striated root connective absent); proximal end of LMR/r1 linked by group of 2–3 fibres to 2–3 triplets of the TB; proximal ends of BBs linked by a striated fibre (*Palatinus*) or without direct connection (*Peridiniopsis*, *Parvodinium*); TMR/r3 extending around TFC (*Peridiniopsis*, *Palatinus*) or

relatively short (*Parvodinium*), nucleating an extension of microtubules (TMRE) toward the dorsal side of the cell; TMRE with about 10–20 microtubules in a flat layer (*Palatinus*, *Parvodinium*) or about 35 proximally and arranged into a circle of 23 microtubules around a fibrous axis distally (*Peridiniopsis*). Distal part of flagellar canals (exit point of each flagellum) surrounded by conspicuous fibrous rings that are connected by one (*Peridiniopsis*, *Parvodinium*) or two fibrous extensions (*Palatinus*); when present, exit point of extended peduncle also surrounded by fibrous ring. Except for a short connective attaching the LMR/r1 of *Peridiniopsis* to the fibrous material that limited the longitudinal flagellar canal, there are no fibres associated with the ventral face of this multistranded root; and there are no dorsal connectives linking the flagellar apparatus to other cytoplasmic structures.

Acknowledgments

Thanks to the Laboratory of Molecular Studies for Marine Environments (LEMAM), where the molecular work was done.

Disclosure statement

No potential conflict of interest was reported by the authors.

Funding

MSP was supported by the grant SFRH/BD/109016/2015 from the financing programs POCH – Programa Operacional Capital Humano and QREN – POPH – Tipologia 4.1 – Formação Avançada, and by the European Social Funding (FSE) and the Portuguese Ministry of Education and Science (MEC). Additional support came from the GeoBioTec Research Unit (UID/GEO/04035/2019) and by national funds (OE), to SCC, through FCT – Fundação para a Ciência e a Tecnologia, I.P., in the scope of the framework contract foreseen in the numbers 4, 5 and 6 of the article 23, of the Decree-Law 57/2016, of 29 August, changed by Law 57/2017, of 19 July.

Supplementary information

The following supplementary material is accessible via the Supplementary Content tab on the article’s online page at <https://doi.org/10.1080/09670262.2022.2091798>

Supplementary figs S1–S4. LM and SEM of *Parvodinium elpatiewskyi* strain from Gafanha da Boavista, Ílhavo. Supplementary fig. S1. Ventral view of a living cell (LM). Nucleus (n), eyespot (e) and radiating chloroplast lobes (ch). Supplementary figs S2, S3. Superficial and deeper focus, from ventral to dorsal view, of an empty theca (LM). Supplementary fig. S4. Apical view of a cell showing the cingulum (c), the apical pore complex (apc) and plates marked in Kofoidian notation (SEM). Cells for SEM observation were fixed for 2 h 30 min in a mixture of 1:1 culture

volume and 50% ethanol. Scale bars: Supplementary figs S1–S3, 10 mm; Supplementary fig. S4, 5 mm.

Supplementary figs S5–S7. *Parvodinium* strain from Buçaco, TEM. Supplementary fig. S5. Longitudinal section of a cell seen from the right-ventral side showing the chloroplast lobes (ch) with some thylakoid-free areas (short black arrows), oil droplets (O), starch grains (st) and trichocysts (t), scattered in the cell periphery. The eyespot (e) is visible in the sulcal region near pusular elements (pu). An almost transverse section of a peduncle (long black arrow) is present outside the cell. Supplementary fig. S6. Magnification of the peduncle displaying a strand of microtubules (thin arrows), and some electron-opaque vesicles (larger arrows). Supplementary fig. S7. Magnification of the eyespot-containing chloroplast lobe with two rows of globules (arrows) with the longitudinal microtubular root (LMR/r1) in the ventral side. Scale bars: Supplementary fig. S5, 2 mm; Supplementary figs S6, S7, 500 nm.

Supplementary figs S8–S11. *Parvodinium* strain from Buçaco, TEM. Longitudinal serial sections through the apical pore complex, viewed from the right-ventral side of the cell. Slanted numbers indicate the section number in the series. Supplementary figs S8, S9. Several striated fibers (long arrows) and a round vesicle (short arrow) are seen under the pore plate (Po). The cover plate (cp) is seen on top of the Po. Supplementary figs S10, S11. Several round and elongated vesicles (short arrows) extend under the Po and converge toward the cp. Scale bars: 500 nm.

Supplementary figs S12–S16. *Parvodinium* strain from Buçaco, TEM. Pusular system and microtubular strand of the peduncle (MSP) in longitudinal serial sections proceeding toward the left-dorsal side, seen from the right-ventral side. Slanted numbers indicate the section number in the series. Supplementary figs S12, S13. The path of the MSP, breached up in several rows of microtubules and marked by arrows, is shown in two sections, the second one, 47 sections towards the left-dorsal side of the cell. In Supplementary fig. S12 the rows of microtubules are closer together and near the network of pusular tubes (PuN). The short arrow points to the apical pore. In Supplementary fig. S13 some rows are visible further up in the epicone, near an accumulation body (ab), while a single row of microtubules is present in the ventral area, near the PuN; the flat pusular vesicle (PuS) is visible on the right side of the cell. Supplementary fig. S14. Magnification of the microtubules and PuN from Supplementary fig. S12. Supplementary figs S15, S16. Magnification from Supplementary fig. S13, of four strands (marked 1–4) of microtubules visible near the ab (Supplementary fig. S15) and the microtubules in the ventral area (Supplementary fig. S16). Electron-opaque bodies are marked by short arrows (Supplementary fig. S15). c, cingulum; O, oil droplets; PuS, pusular sheet; s, sulcus; st, starch grains. Scale bars: Supplementary figs S12, S13, 5 mm; Supplementary figs S14–S16, 500 nm.

Supplementary Figs S17–S19. *Parvodinium* strain from Buçaco, TEM. Pusular system and microtubular strand of the peduncle (MSP); continuation of the series of sections shown in Figs 24, 25. Supplementary fig. S17. General view showing the descending path of the microtubular strand of the peduncle after inflecting to the left side of the cell (thin arrows). The pusular network (PuN) and pusular sheet (PuS) are visible on the ventral-right side of the cell. A transverse section through a detached peduncle (short arrow) is visible outside the cell, on the ventral side, near the sulcus (s). Supplementary fig. S18. Magnification of Supplementary fig. S17 showing four

rows of microtubules from the MSP and electron-opaque bodies (short arrows). Supplementary fig. S19. Magnification of the PuS from Supplementary fig. S17 containing electron-opaque bodies (black arrows) and a tubular portion with dot-like contents reminiscent of the pusular tube associated with the TFC (white arrow). c, cingulum; e, eyespot; O, oil droplets; s, sulcus; st, starch grains. Scale bars: Supplementary fig. S17, 5 mm; Supplementary figs S18, S19, 500 nm.

Supplementary Fig. S20. Concatenated phylogeny based on 3923 base pairs of large subunit rDNA, internal transcribed spacers, 5.8S rDNA and small subunit rDNA of 12 genera of Dinophyceae (27 sequences) and inferred from Bayesian analysis. For this analysis *Heterocapsa* spp. were used as outgroup taxa. Branch support was evaluated from posterior probabilities (probabilities (PP) ≥ 0.5) from Bayesian analyses and bootstrap (1000 replications, BS $\geq 50\%$) from maximum likelihood analyses, respectively. These support values are written at internodes. A hyphen (-) indicates values below 0.5 for PP and 50% for bootstrap. GenBank accession numbers are written after the species epithet. Sequences determined in this study were bold faced. The branch lengths are proportional to the number of character changes, see scale bar below the phylogenetic tree.

Author contributions

M.S. Pandeirada: LM, TEM and SEM preparation and analysis, molecular analyses, drafting manuscript; S.C. Craveiro: TEM preparation, molecular analyses, drafting manuscript; N. Daugbjerg: phylogenetic analyses, drafting and editing manuscript; Ø. Moestrup: editing manuscript; A.J. Calado: original concept, TEM analysis, editing manuscript.

ORCID

Mariana S. Pandeirada  <http://orcid.org/0000-0001-5061-9029>
Sandra C. Craveiro  <http://orcid.org/0000-0002-2738-7626>
Niels Daugbjerg  <http://orcid.org/0000-0002-0397-3073>
Øyvind Moestrup  <http://orcid.org/0000-0003-0965-8645>
António J. Calado  <http://orcid.org/0000-0002-9711-0593>

References

- Andersen, R.A., Berges, J.A., Harrison, P.J. & Watanabe, M. (1997). Recipes for freshwater and seawater media. In *Algal Culturing Techniques* (Andersen, R.A., editor), 429–538. Elsevier Academic Press, Burlington, MA.
- Calado, A.J. (2011). On the identity of the freshwater dinoflagellate *Glenodinium edax*, with a discussion on the genera *Tyrannodinium* and *Katodinium*, and the description of *Opisthoaulax* gen. nov. *Phycologia*, **50**: 641–649.
- Calado, A.J. & Moestrup, Ø. (1997). Feeding in *Peridiniopsis berlinensis* (Dinophyceae): new observations on tube feeding by an omnivorous, heterotrophic dinoflagellate. *Phycologia*, **36**: 47–59.
- Calado, A.J. & Moestrup, Ø. (2002). Ultrastructural study of the type species of *Peridiniopsis*, *Peridiniopsis borgei* (Dinophyceae), with special reference to the peduncle and flagellar apparatus. *Phycologia*, **41**: 567–584.

- Calado, A.J., Craveiro, S.C. & Moestrup, Ø. (1998). Taxonomy and ultrastructure of a freshwater, heterotrophic *Amphidinium* (Dinophyceae) that feeds on unicellular protists. *Journal of Phycology*, **34**: 536–554.
- Calado, A.J., Hansen, G. & Moestrup, Ø. (1999). Architecture of the flagellar apparatus and related structures in the type species of *Peridinium*, *P. cinctum* (Dinophyceae). *European Journal of Phycology*, **34**: 179–191.
- Carty, S. (2008). *Parvodinium* gen. nov. for the Umbonatum group of *Peridinium* (Dinophyceae). *Ohio Journal of Science*, **108**: 103–107.
- Craveiro, S.C., Calado, A.J., Daugbjerg, N. & Moestrup, Ø. (2009). Ultrastructure and LSU rDNA-based revision of *Peridinium* group palatinum (Dinophyceae) with the description of *Palatinus* gen. nov. *Journal of Phycology*, **45**: 1175–1194.
- Craveiro, S.C., Calado, A.J., Daugbjerg, N., Hansen, G. & Moestrup, Ø. (2011). Ultrastructure and LSU rDNA-based phylogeny of *Peridinium lomnickii* and description of *Chimonodinium* gen. nov. (Dinophyceae). *Protist*, **162**: 590–615.
- Craveiro, S.C., Pandeirada, M.S., Daugbjerg, N., Moestrup, Ø. & Calado, A.J. (2013). Ultrastructure and phylogeny of *Theleodinium calcisporum* gen. et sp. nov., a freshwater dinoflagellate that produces calcareous cysts. *Phycologia*, **52**: 488–507.
- Craveiro, S.C., Daugbjerg, N., Moestrup, Ø. & Calado, A.J. (2015). Fine-structural characterization and phylogeny of *Peridinium polonicum*, type species of the recently described genus *Naiadinium* (Dinophyceae). *European Journal of Protistology*, **51**: 259–279.
- Craveiro, S.C., Daugbjerg, N., Moestrup, Ø. & Calado, A.J. (2016). Studies on *Peridinium aciculiferum* and *Peridinium malmogiense* (= *Scrippsiella hangoei*): comparison with *Chimonodinium lomnickii* and description of *Apocalathium* gen. nov. (Dinophyceae). *Phycologia*, **56**: 21–35.
- Elbrächter, M. & Meyer, B. (2001). Plate pattern variability and plate overlap in a clonal culture of the freshwater dinoflagellate *Peridinium umbonatum* Stein species complex (Dinophyceae). *Neues Jahrbuch für Geologie und Paläontologie/Abhandlungen*, **219**: 221–227.
- Gottschling, M., Kretschmann, J. & Žerdoner Čalasan, A. (2017). Description of Peridiniopsidaceae, fam. nov. (Peridinales, Dinophyceae). *Phytotaxa*, **299**: 293–296.
- Guindon, S., Dufayard, J.F., Lefort, V., Anisimova, M., Hordijk, W. & Gascuel, O. (2010). New algorithms and methods to estimate maximum-likelihood phylogenies: assessing the performance of PhyML 3.0. *Systematic Biology*, **59**: 307–321.
- Hansen, P.J. & Calado, A.J. (1999). Phagotrophic mechanisms and prey selection in free-living dinoflagellates. *Journal of Eukaryotic Microbiology*, **46**: 382–389.
- Hansen, G., Moestrup, Ø. & Roberts, K.R. (1996). Fine structural observations on *Gonyaulax spinifera* (Dinophyceae), with special emphasis on the flagellar apparatus. *Phycologia*, **35**: 354–366.
- Hansen, G., Daugbjerg, N. & Henriksen, P. (2007). *Baldinia anauniensis* gen. et sp. nov.: a ‘new’ dinoflagellate from Lake Tovel, N. Italy. *Phycologia*, **46**: 86–108.
- Horiguchi, T. & Chihara, M. (1983). *Scrippsiella hexapraecingula* sp. nov. (Dinophyceae), a tide pool dinoflagellate from the Northwest Pacific. *The Botanical Magazine, Tokyo*, **96**: 351–358.
- Horiguchi, T., Kawai, H., Kubota, M., Takahashi, T. & Watanabe, M. (1999). Phototactic responses of four marine dinoflagellates with different types of eyespot and chloroplast. *Phycological Research*, **47**: 101–107.
- Huber-Pestalozzi, G. (1950). Das Phytoplankton des Süßwassers. Systematik und Biologie. 3. Teil. Cryptophyceen, Chloromonaden, Peridineen. In *Die Binnengewässer ...* (Thienemann, A., editor) vol. **16**. E. Schweizerbart’sche Verlagsbuchhandlung, Stuttgart. IX + 310 pp.
- Iwataki, M., Hansen, G., Moestrup, Ø. & Matsuoka, K. (2010). Ultrastructure of the harmful unarmored dinoflagellate *Cochlodinium polykrikoides* (Dinophyceae) with reference to the apical groove and flagellar apparatus. *Journal of Eukaryotic Microbiology*, **57**: 308–321.
- Kretschmann, J., Owsianny, P.M., Žerdoner Čalasan, A. & Gottschling, M. (2018). The hot spot in a cold environment: puzzling *Parvodinium* (Peridiniopsidaceae, Peridinales) from the Polish Tatra mountains. *Protist*, **169**: 206–230.
- Kretschmann, J., Žerdoner Čalasan, A., Meyer, B. & Gottschling, M. (2019). Zero intercalary plates in *Parvodinium* (Peridiniopsidaceae, Peridinales) and phylogenetics of *P. elpatiewskyi*, comb. nov. *Protist*, **171**: Article 125700.
- Lefèvre, M. (1932). Monographie des espèces d’eau douce du genre *Peridinium*. *Archives de Botanique*, **2 (Mémoire 5)**: 1–210.
- Lemmermann, E. (1899). Ergebnisse einer Reise nach dem Pacific. H. Schauinsland 1896/97. *Abhandlungen herausgegeben vom Naturwissenschaftlichen Verein zu Bremen*, **16**: 313–398, pls I–III.
- Lemmermann, E. (1905). Die Algenflora der Sandwich-Inseln. Ergebnisse einer Reise nach dem Pacific. H. Schauinsland 1896/97. *Botanische Jahrbücher für Systematik Pflanzengeschichte und Pflanzengeographie*, **34**: 607–663, pls VII–VIII.
- Lemmermann, E. (1910). *Algen I (Schizophyceen, Flagellaten, Peridineen)*. Kryptogamenflora der Mark Brandenburg, Bd. 3. Gebrüder Borntraeger, Leipzig, 712 pp.
- Lindberg, K., Moestrup, Ø. & Daugbjerg, N. (2005). Studies on woloszynskioid dinoflagellates I: *Woloszynskia coronata* re-examined using light and electron microscopy and partial LSU rDNA sequences, with description of *Tovellia* gen. nov. and *Jadwigia* gen. nov. (Tovelliaceae fam. nov.). *Phycologia*, **44**: 416–440.
- Lindström, K. (1991). Nutrient requirements of the dinoflagellate *Peridinium gatumense*. *Journal of Phycology*, **27**: 207–219.
- Ling, H.U., Croome, R.L. & Tyler, P.A. (1989). Freshwater dinoflagellates of Tasmania, a survey of taxonomy and distribution. *British Phycological Journal*, **24**: 111–129.
- Litaker, R.W., Vandersea, M.W., Kibler, S.R., Madden, V.J., Noga, E.J. & Tester, P.A. (2002). Life cycle of the heterotrophic dinoflagellate *Pfiesteria piscicida* (Dinophyceae). *Journal of Phycology*, **38**: 442–463.
- Logares, R., Shalchian-Tabrizi, K., Boltovskoy, A. & Rengefors, K. (2007). Extensive dinoflagellate phylogenies indicate infrequent marine-freshwater transitions. *Molecular Phylogenetics and Evolution*, **45**: 887–903.
- Luo, Z., Mertens, K.N., Nézan, E., Gu, L., Pospelova, V., Thoha, H. & Gu, H. (2019). Morphology, ultrastructure and molecular phylogeny of cyst-producing *Caladoa arcachonensis* gen. et sp. nov. (Peridinales, Dinophyceae) from France and Indonesia. *European Journal of Phycology*, **54**: 235–248.
- Luo, Z., Mertens, K.N., Gu, H., Wang, N., Wu, Y., Uttayarnmanee, P., Pransilpa, M. & Roeroe, K.A. (2020). Morphology, ultrastructure and molecular phylogeny of

- Johsia chumphonensis* gen. et sp. nov. and *Parvodinium parvulum* comb. nov. (Peridiniopsidaceae, Dinophyceae). *European Journal of Phycology*, **56**: 324–336.
- Messer, G. & Ben-Shaul, Y. (1969). Fine structure of *Peridinium westii* Lemm., a freshwater dinoflagellate. *Journal of Protozoology*, **16**: 272–280.
- Moestrup, Ø. (2000). The flagellate cytoskeleton. Introduction of a general terminology for microtubular flagellar roots in protists. In *The Flagellates. Unity, Diversity and Evolution* (Leadbeater, B.S.C. & Green, J. C., editors), 69–94. (Systematics Association Special Volume No. 59). Taylor & Francis, New York.
- Moestrup, Ø. & Daugbjerg, N. (2007). On dinoflagellate phylogeny and classification. In *Unravelling the Algae: The Past, Present, and Future of Algae Systematics* (Brodie, J. & Lewis, J., editors), 215–230. (Systematics Association Special Volume No. 75). CRC Press, Boca Raton.
- Moestrup, Ø. & Calado, A.J. (2018). Dinophyceae. In *Süßwasserflora von Mitteleuropa – Freshwater Flora of Central Europe* (Büdel, B., Gärtner, G., Krienitz, L. & Schagerl, M., editors), vol. 6, 2nd edition. Springer-Verlag, Berlin. XII + 561 pp.
- Pandeirada, M.S., Craveiro, S.C., Daugbjerg, N., Moestrup, Ø., Domingues, P. & Calado, A.J. (2019). Studies on woloszynskioid dinoflagellates X: ultrastructure, phylogeny and colour variation in *Tovellia rubescens* sp. nov. (Dinophyceae). *Journal of Eukaryotic Microbiology*, **66**: 937–953.
- Pandeirada, M.S., Craveiro, S.C., Daugbjerg, N., Moestrup, Ø. & Calado, A.J. (2021). Fine-structural characterization and phylogeny of *Sphaerodinium* (Suessiales, Dinophyceae), with the description of an unusual type of freshwater dinoflagellate cyst. *European Journal of Protistology*, **78**: Article 125770.
- Popovský, J. & Pfister, L.A. (1986). A taxonomical note to the section *umbonatum* of the genus *Peridinium* Ehrenberg, 1932 (Dinophyceae). *Archiv für Protistenkunde*, **132**: 73–77.
- Popovský, J. & Pfister, L.A. (1990). Dinophyceae (Dinoflagellida). In *Süßwasserflora von Mitteleuropa* (Ettl, H., Gerloff, J., Heynig, H. & Mollenhauer, D., editors), vol. 6. Gustav Fischer, Jena.
- Pandeirada, M.S., Craveiro, S.C., Daugbjerg, N., Moestrup, Ø. & Calado, A.J. (2014). Studies on woloszynskioid dinoflagellates VI: description of *Tovellia aveirensis* sp. nov. (Dinophyceae), a new species of Tovelliaceae with spiny cysts. *European Journal of Phycology*, **49**: 230–243.
- Pandeirada, M.S., Craveiro, S.C., Daugbjerg, N., Moestrup, Ø. & Calado, A.J. (2017). Studies on woloszynskioid dinoflagellates VIII: life cycle, resting cyst morphology and phylogeny of *Tovellia rinoi* sp. nov. (Dinophyceae). *Phycologia*, **56**: 533–548.
- Playfair, G.I. (1920). Peridineae of New South Wales. *Proceedings of the Linnean Society of New South Wales*, **44**: 793–818, pls XLI–XLIII.
- Roberts, K.R., Timpano, P. & Montegut, A.E. (1987). The apical fibrous complex: a new cytological feature of some dinoflagellates. *Protoplasma*, **137**: 65–69.
- Ronquist, F. & Huelsenbeck, J.P. (2003). MrBayes 3: Bayesian phylogenetic inference under mixed models. *Bioinformatics*, **19**: 1572–1574.
- Saldarriaga, J.F., Taylor, F.J.R., Keeling, P.J. & Cavalier-Smith, T. (2001). Dinoflagellate nuclear SSU rRNA phylogeny suggests multiple plastid losses and replacements. *Journal of Molecular Evolution*, **53**: 204–213.
- Schiller, J. (1935). Dinoflagellatae (Peridineae) in monographischer Behandlung. In *Rabenhorst's Kryptogamenflora von Deutschland, Österreich und der Schweiz*, 2nd edition, **10** (3). Part 2, Issue 2. (Kolkwitz, R., editor), 161–320. Akademische Verlagsgesellschaft, Leipzig.
- Schilling, A.J. 1891. Die Süßwasser-Peridineen. *Flora*, **74**: 220–299, pls VIII–X.
- Schnepf, E., Deichgräber, G. & Drebes, G. (1985). Food uptake and the fine structure of the dinophyte *Paulsenella* sp., an ectoparasite of marine diatoms. *Protoplasma*, **124**: 188–204.
- Seo, K.S. & Fritz, L. (2002). Diel changes in pyrenoid and starch reserves in dinoflagellates. *Phycologia*, **41**: 22–28.
- Starmach, K. (1974). Cryptophyceae, Dinophyceae, Raphidophyceae. In *Flora Słodkowodna Polski* (Starmach, K. & Siemińska, J., editors), vol. 4. Państwowe Wydawnictwo Naukowe, Warszawa, Kraków. 520 pp.
- Stein, F. (1883). *Der Organismus der Infusionsthier nach eigenen Forschungen in systematischer Reihenfolge bearbeitet. III. Abtheilung. Die Naturgeschichte der Flagellaten oder Geißelinfusorien. II. Hälfte. Die Naturgeschichte der arthrodelen Flagellaten. Einleitung und Erklärung der Abbildungen.* Wilhelm Engelmann, Leipzig. 30 pp, XXV pls.
- Stern, R.F., Andersen, R.A., Jameson, I., Küpper, F.C., Coffroth, M.-A., Vaultot, D., Le Gall, F., Véron, B., Brand, J.L., Skelton, H., Kasai, F., Lilly, E.L. & Keeling, P.J. (2012). Evaluating the ribosomal Internal Transcribed Spacer (ITS) as a candidate dinoflagellate barcode marker. *PLoS ONE*, **7**: Article e42780.
- Swofford, D.L. (2002). *PAUP*. Phylogenetic Analysis Using Parsimony (* and Other Methods)*. Version 4. Sinauer Associates, Sunderland, MA.
- Takano, Y. & Horiguchi, T. (2005). Acquiring scanning electron microscopical, light microscopical and multiple gene sequence data from a single dinoflagellate cell. *Journal of Phycology*, **42**: 251–256.
- Waterhouse, A.M., Procter, J.B., Martin, D.M.A., Clamp, M. & Barton, G.J. (2009). Jalview Version 2 – a multiple sequence alignment editor and analysis workbench. *Bioinformatics*, **25**: 1189–1191.
- Zhang, Q., Liu, G-X. & Hu, Z-Y. (2011). Morphological observation of a freshwater *Peridinium* strain and phylogenetic analysis of *Peridinium*. *Plant Science Journal*, **29**: 1–10.